Thermal versus mechanical topography: An experimental investigation in a rotating baroclinic annulus

S. D. Marshall* and P. L. Read

Atmospheric, Oceanic and Planetary Physics, Clarendon Laboratory, University of Oxford, Parks Road, Oxford, OX1 3PU, UK

(Received ?????; in final form ?????; first published online ?????)

We present a series of experimental investigations in which a differentially-heated annulus was used to investigate the effects of topography on rotating, stratified flows. In particular, we investigate blocking effects via azimuthally varying differential-heating and compare them to previous experiments utilising partial mechanical barriers (Marshall and Read, *Geophys. Astrophys. Fluid Dyn.* 2018, **112**).

The thermal topography used consisted of a flat patch of heating elements covering a small azimuthal extent of the base, forming an equivalent of a partial barrier, to study the difference between blocked and unblocked flow. These azimuthally-varying heating experiments produced results with many similarities to our previous experiments with a mechanical barrier, despite the lack of a physical obstacle or formation of bottom-trapped waves. In particular, a unique flow structure was found when the drifting flow and the topography interacted in the form of an 'interference' regime at low Taylor number, but forming an erratic 'irregular' regime at higher Taylor number. This suggests that blocking may be induced by either or both of a thermal or mechanical inhomogeneity. Evidence of coherent/persistent resonant wave triads was noted in both kinds of experiment, though the component wavenumbers of the wave-triads and their impact on the flow was found to depend on the topography in question.

Keywords: Topography; Annulus; Blocking, Wave-Triads; Trapped Waves.

1. Introduction

The various influences of mechanical topography on the atmospheric circulation, such as determining the existence and location of stationary topographic waves superposed on the zonal flow, have been repeatedly studied in detail, as in e.g. Charney and DeVore (1979), Li, Kung and Pfeffer

*Corresponding Author. Present Address: Department of Mechanical Engineering, National University of Singapore, 117575, Singapore. Email: mpesdm@nus.edu.sg

(1992), and Read and Risch (2011). Another type of stationary perturbation to the large-scale flow, equivalent to topographic barriers or obstacles but relatively less frequently discussed in the atmospheric sciences literature, is that of 'thermal topography' – associated with the presence of differential heating in the zonal direction, in addition to meridionally-varying heating between the equator and poles. Such thermal topography may arise on the Earth due to the thermal differences between continental scale land masses and the sea. This effect is felt most strongly in the tropics, where the large-scale flow generated is known as the Walker Circulation (hereafter WC), as discussed e.g. by Bjerknes (1969). Due to its comparative weakness throughout most of the year, the WC is not as well understood as more prominent atmospheric circulation patterns such as the Hadley Cell. However, Boubnov, Golitsyn and Senatorsky (1991) note that, during the winter, "the temperature contrast between continents and oceans is of the same order as the temperature difference between tropical and polar regions." As touched upon by Georgen and Lin (2002), it is an interesting question as to whether, and in what way, thermal topography can be thought of as a parallel to mechanical (i.e. non-thermal) topography, and whether there is a direct comparison to be found between the two.

Such effects may be even more important in the atmosphere of Mars, whose surface includes continental-scale mountain ranges and plateaux of large amplitude. The radiative balances between atmosphere and surface on Mars differ markedly from those on Earth, because the Martian atmosphere is relatively thin and composed mostly of CO_2 (for example see Read and Lewis 2004). As a result, large-scale, high altitude topographic relief may also lead to strong inhomogeneities in radiative heating or cooling at a given altitude or pressure level (e.g. Nayvelt, Gierasch and Cook 1997) and so topography on Mars has both a mechanical and thermal effect on the atmosphere above. It remains to be determined, therefore, which type of forcing has a greater impact on the general circulation, under given conditions.

The concept of thermal topography may also be in some manner related to the possible origins of current 'extreme weather' conditions associated with climate change. Studies such as those of Francis and Vavrus (2012) and Liu *et al.* (2012), for example, conclude that a reduction in Arctic sea-ice from global warming has led to significant changes to the atmospheric circulation. Francis and Vavrus

suggest that the resulting smaller land-sea temperature difference has led to a slower eastward progression of Rossby waves due to weakened zonal winds, and increased wave amplitudes. Liu *et al.* note how this links to the impacts of blocking, and thus propose that a lack of sea-ice may lead to more frequent blocked states, in turn leading to cold surges and perhaps at least partially accounting for the "recent cold and snowy winters".

In order to investigate mechanical and thermal topographic impacts, a differentially-heated annulus experiment with topography (as discussed in Hide and Mason 1975, Weeks *et al*. 1997, and Read and Risch 2011, for example) enables the production of controllable baroclinic flows in a laboratory environment, and will form the framework of the experiments conducted here. The experimental arrangement is similar in design to that of another work, Marshall and Read (2018), which utilised an isolated ridge to create a mechanical topographic partial barrier to the flow. Here we impose a local heating anomaly to the flow and make clear comparisons and contrasts between the respective effects of thermal and mechanical topography.

1.1. Thermal topography in geophysical flows

Studies of the impact of varying land-sea temperature contrasts first began when Bjerknes (1969) discovered that the strength of the WC was dependent on sea-surface temperatures (SSTs), being stronger when the temperatures were lower and weaker when they were higher. Since the WC is caused by differences between SSTs and those of the land surface in the tropics, this circulation is also closely linked with the El Niño Southern Oscillation (hereafter ENSO), a chaotic oscillation with a recurrence timescale on the order of 3-6 years. ENSO is defined by Philander (1985) as representing irregular cyclic periods of warming (El Niño) and cooling (La Niña) of the eastern Pacific tropics. Power and

Smith (2007), amongst others, noted that the observed weakening of the WC, which they attributed to global warming reducing the land-sea temperature difference, may be happening at the same time as an increasing dominance of ENSO in the Southern Hemisphere. With the WC and the previously discussed Arctic sea-ice problem both being strongly related to concerns about climate change, an understanding of the issue of thermal topography and its impact on the global circulation is thus becoming increasingly important. It is important to note that the effects of the WC can also be found outside of the tropics (as discussed e.g. by Shulmeister 1999), with Meehl (1994), amongst others, linking mid-latitude land-sea temperature differences to the formation of monsoons and associated circulations. This being the case, it is apparent that the main driving factors of the WC are not reliant on it being tropical, but instead that the essential feature is a notable horizontal temperature difference. In this way the baroclinic annulus experiment, which more strongly resembles the atmospheric circulation of the mid-latitudes than the tropics, can be employed to study the WC if an equivalent horizontal temperature contrast can be replicated.

As well as land-sea temperature differences, thermal topography can also arise from geothermal or volcanic action, especially in the open ocean. For example, Mashayek *et al.* (2013), via observations and numerical simulations, found that the impact of a geothermal heat flux at the ocean bottom could lead to a reduction in the weakly stable stratification throughout the abyssal layer, resulting in a strengthening of the circulation. The authors argue that geothermal heat flux may therefore be a vital component for inclusion into oceanic modelling. To examine whether the thermal topographic experiments can replicate this effect, and thus give insights into the impact of geothermal heat flux in general, signs of vertical uniformity were searched for in our present experiments, especially in comparison to other studies without azimuthally-varying heating. Once again, this also allows the current investigation to extend its focus to consider oceanic flows, as well as atmospheric circulations.

As mentioned previously, thermal topography also has links to the Martian atmospheric circulation, with Nayvelt, Gierasch and Cook (1997) noting that, away from the poles and in the absence of a global dust storm, the Martian diabatic heating at the surface is dominated by direct radiative exchanges to space, with very little atmospheric sensible or latent heating of the surface compared to

Earth, where the surface temperature of topographic peaks is approximately the same as the temperature of the atmosphere at that height. In contrast, Webster (1977) found that topographic features of the Martian surface tend to have a uniform surface temperature, regardless of their height. In this way Martian surface topographic features can effectively act as atmospheric heat sources at their peaks and heat sinks within troughs, as well as functioning as mechanical obstacles.

Due to this effect, Mars and Earth may have differing linear stationary responses, with the former experiencing "global, low wavenumber responses". This has been backed up both by the numerical studies of Webster (1977) and Hollingsworth and Barnes (1995), and by observations, such as from Banfield *et al.* (1996), who found low wavenumber disturbances across the global scale (wavenumber-1 and wavenumber-2 in the observations). These disturbances have been linked to the formation of robust stationary eddies (and hence, influencing the location and occurrence of global dust storms, as discussed earlier) in the Martian atmosphere, especially in the Northern Hemisphere. In our Thermal Topography experiments presented here, therefore, we examine how much local thermal forcing contributes towards the generation of large-scale stationary structures, especially in comparison to the effects of mechanical topographic forcing investigated in previous studies.

As described by Marshall and Read (2018), a major influence of mechanical topography on the atmospheric circulation is the formation of distinct, stable circulation regimes, leading to the development of either a "blocked" flow or a "zonal" flow as alternative states, depending upon initial conditions. Both of these states may be stable at the same location in parameter space (sometimes also referred to as *metastable* or *quasi-stable*), giving rise to the existence of multiple equilibria or other forms of multi-stability. In addition, Weeks *et al.* (1997) noted that blocking events ("persistent blocking anomalies") typically occur over a timescale of 10-100 days, which happens to be the same as that of more general atmospheric low frequency variability (LFV). This implies that transitions between *blocked* and *zonal* states are likely to be associated with the mechanism that leads to the occurrence of LFV in the atmosphere. Marshall and Read (2018) found evidence of blocking states in a baroclinic

annulus with aperiodic mechanical topography, and it is suggested that thermal topography would also be able to produce similar results. It is well known from linear theory (e.g. Holton 1992 and Pedlosky 1987) that both thermal forcing and topographic forcing are able to produce either vertically trapped waves or strongly vertically propagating waves, depending upon the stratification and horizontal wavenumber. In this way, Boubnov, Golitsyn and Senatorsky (1991) investigated effects of thermal topography in the laboratory by imposing azimuthally-varying heating in an annulus with four discrete segments in their outer cylinder, as opposed to a single continuous one. Not only were baroclinic waves encountered, but the results of the investigation demonstrated drifting waves that interacted with the heaters as they moved past them. Stationary waves were found, along with a reduction in the strength of the zonal flow, suggesting an appearance of blocking effects. These findings imply a similarity between thermal and mechanical topography, as the flow evidently reacted in a manner that would also be expected with a mechanical barrier imposed at the lower boundary.

It is therefore hoped that the present investigation may improve knowledge of this topic, by, for example, conducting experiments with azimuthally-varying heating over the same range of parameter space and with a similar layout as for the experiments with mechanical topography of Marshall and Read (2018). Marshall and Read employed an isolated ridge of mechanical topography, creating a vertical partial barrier, and noted evidence of topographically induced oscillations between stationary and drifting waves in an 'interference' region. At higher rotation rates, an 'irregular' region of erratic flow structure was found, associated with the occurrence of resonant wave-triads between the topographically-forced stationary wave and higher wavenumber drifting waves. In addition, unlike Read and Risch (2011, 2015), Marshall and Read (2018) found no evidence of multiple equilibria. It is of interest whether the present thermal topography can reproduce these findings, in particular the occurrence of topographic interactions and distinct regions of flow behaviour, as well as the absence of multiple equilibria. In this way, and to allow study of any other differences to the flow structure and evolution caused by thermal topography, frequent comparison will be made between Marshall and Read's results and those presented here. As well as providing a parallel to mechanical topography, azimuthally-varying heating also helps to create a "less-idealised" annulus, which takes account of the

temperature differences both between the equator and the poles and between the continental landmasses and the ocean in the Earth's climate system. Local bottom heating will tend to reduce low level static stability and perhaps even induce local convection and a secondary circulation, in contrast to a purely mechanical obstacle that just deflects the flow upwards or horizontally around the obstacle. In this way the influence of the topography may be extended further from the heat source than from a localised ridge, and could hence make the far field interaction more complicated.

1.2. Outline

Section 2 presents a detailed account of the experimental apparatus that this project utilised, as well as the methodology that was employed, and defines some of the key dimensionless numbers needed to describe the most relevant parameter space. Section 3 provides the results of the conducted experiments, including analysis of the results gathered. This is followed by a discussion and summary of conclusions, section 4, and examines how successful the investigation has been at achieving the aims and objectives set out in the previous section and discuss the physical implications of the results gathered.

2. Experimental arrangement

2.1. Non-dimensional numbers

Whilst the circulation of a planetary atmosphere is extremely complicated and depends on a large number of parameters, the principal flow regimes in typical rotating annulus experiments are generally characterised mainly by two dimensionless numbers defining a tractable parameter space. The Taylor Number for an annulus experiment (as described in Fowlis and Hide 1965) is defined as:

$$\mathcal{T} = \frac{4\Omega^2(b-a)^5}{\nu^2 d}, \tag{1}$$

where ν is the kinematic viscosity, a is the inner radius, b is the outer radius, d is the height of the annulus and Ω is the rate of rotation of the annulus. Roughly, the Taylor Number gives the squared ratio of the Coriolis forces (the numerator) to the viscous forces (the denominator) acting upon a fluid. A large value implies a less strongly damped flow, with circulation in the annulus effectively tending toward a broader spectrum of dominant wavenumbers and ultimately the irregular regime.

Secondly, the Hide Number (sometimes also known as the Thermal Rossby Number, such as in Hide 1958, Hide and Mason 1975 and Read *et al*. 2015, amongst others) for an annulus experiment is defined as:

$$\Theta_T = \frac{\alpha g d \Delta T}{\Omega^2(b-a)^2}, \tag{2}$$

where α is the thermal expansion coefficient, g is the gravitational acceleration and ΔT is the temperature difference. A full derivation can be found in Holton (1992), for example. Roughly, the Hide Number gives the ratio of the inertial forces (the numerator) to the Coriolis forces (the denominator) acting upon a fluid, with a scaling velocity determined by the typical thermal wind shear.

For an annulus experiment (or similar) the rotation rate and the temperature difference are the main sources of control. Hence, together with the Prandtl number (kept constant in the present investigation), these dimensionless numbers can be taken to adequately describe the parameter space within which the experiments take place (as in Hide and Mason 1975, Weeks *et al*. 1997, Read and Risch 2011 and Read *et al.* 2015, amongst others).

2.2. Equipment description

Accounts of the experimental arrangement in question can be found more fully in Wordsworth, Read and Yamazaki (2008), Marshall and Read (2015), and Marshall and Read (2018). Its dimensions, as well as several other relevant experimental parameters, are given in Table 1.

Table 1: Important experimental parameters

Radius of Inner Cylinder	a	4.5 ± 0.05 cm
Radius of Outer Cylinder	b	14.3 ± 0.05 cm
Depth of Annulus	d	26.5 ± 0.05 cm
Density of Water-Glycerol Mixture at 20°C	ρ_g	1044 ± 0.5 kgm^{-3}
Kinematic Viscosity of Water-Glycerol Mixture at 20°C	ν_g	$1.58x10^{-6} \pm 3 \times 10^{-8}$ m^{2}s^{-1}
Thermal Expansion Coefficient of Water-Glycerol Mixture at 20°C	α_g	$3.16x10^{-4} \pm 1 \times 10^{-6}$ K^{-1}

The working fluid is a mixture of water and glycerol, made up so that its density is 1044 ± 0.5 kg m^{-3}, and its kinematic viscosity is $1.58 \pm 0.03 \times 10^{-6}$ m^{2}s^{-1}. This density allows 350-500 μm diameter pliolite tracer particles to be neutrally buoyant. For visualisation, an array of strips of Maxilux Prostrip 120 white light LEDs, arranged over five layers surrounded the annulus, allow light to pass through transparent slits to form flat, collimated light sheets at those layers. This arrangement is illustrated in figure 1. A camera is mounted above the annulus on a tripod-shaped superstructure, with a cone blocking all outside light between it and the acrylic lid. With this arrangement the camera can see the motion of the tracer particles, and thus the flow structure, at any one of the five levels. By switching quickly between the layers the vertical structure can also be resolved.

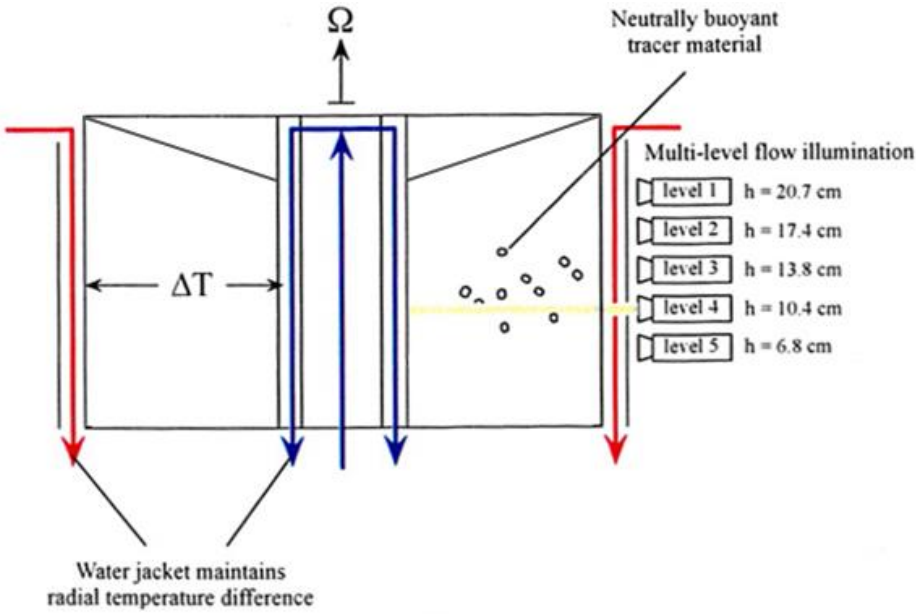

Figure 1: Schematic of the lighting array, sloped lid and heating system in side view (colour online, reproduced from Wordsworth *et al.* 2008, with the permission of AIP Publishing).

2.2.1. Data acquisition

A Firewire (type: DFK 31BF03) camera, chosen due to its high picture quality and lossless compression, was attached to a Lenovo ThinkPad SL510 laptop, using MATLAB as a framework for all camera functions. MATLAB's Image Acquisition Toolbox was employed to create real-time streakline images and movies, for characterisation of the flow type and structure, as well as individual frame-by-frame images. The Firewire camera was set to use a frame-rate of 3.75 frames/second for flow visualisation and it was found that the optimal streakline images were made via 11 captures with a 3 frame interval between each, giving effective streaks of roughly 8.8 seconds. The frame-by-frame images were then analysed using Correlation Image Velocimetry (CIV), as described by Fincham and Spedding (1997), for example. From this information, vector velocity field measurements of the flow were obtained by CIV and then further analysed, giving a detailed examination of the flow structure, including an azimuthal Fourier decomposition. For this software, the uncertainty in image location is given as ± 0.2 pixels, which corresponds to ± 0.04 mm. As such, the absolute uncertainty in velocity can be calculated by dividing this value by the time step between frames ($0.2\dot{6}$ s), giving an error of 0.15 mm/s.

2.2.2. Thermal and mechanical topographic design

A transparent, acrylic, conically-sloping lid was placed in contact with the fluid, as also used in related studies in the same apparatus (Wordsworth, Read and Yamazaki 2008 and Marshall and Read 2015, 2018), with a 22° slope on the bottom and 3.5° slope on the top, to correct for optical distortions at the set camera height. Under a sloped lid it was found to be easier to find resonant wave patterns, as the topographic beta effect that is added by the sloping boundary to the fluid acts to slow down the drift of the waves relative to the apparatus. As such, stationary structures, and in turn topographic resonance, were found to occur more readily in the examined parameter space and at lower Taylor Numbers. The experiments were run with a lid that sloped downwards towards the centre, and with a heated inner cylinder and cooled outer cylinder, which is the reverse of more typical rotating annulus experiments (see e.g. Hide and Mason 1975). This configuration was used so that the lid sloped in the same direction as the isotherms, thereby both increasing the instability of the freely evolving baroclinic waves and enabling their azimuthal phase propagation to become roughly stationary relative to the walls of the annulus (as discussed by Mason 1975). The latter was necessary in order to promote a near-resonant response to the stationary quasi-wavenumber-1 thermal bottom topography.

To achieve the azimuthally-varying heating profile needed to produce some thermal topography, electrical heating elements were attached to the (flat) base of the annulus. These elements were stretched from the inner to the outer wall over a sector corresponding to one third of the area of the base, roughly corresponding to the area occupied by a single peak of the mechanical topography used in the partial barrier experiments of Marshall and Read (2018). This arrangement was chosen to allow a direct comparison between flows found in the Thermal Topography experiments and those using the isolated ridge, especially with regard to the question of whether blocking features can occur as a result of thermal perturbations, without the presence of a physical peak obstructing the flow. The voltage across the elements could be adjusted, allowing a range of possible input heat fluxes to be

imposed while also retaining control over the imposed thermal gradient between inner and outer sidewall. Three rectangular elements of 3 cm by 10 cm were utilised; each rated at 10 W/in^2 (1.55 W/cm^2). The arrangement is shown in figure 2.

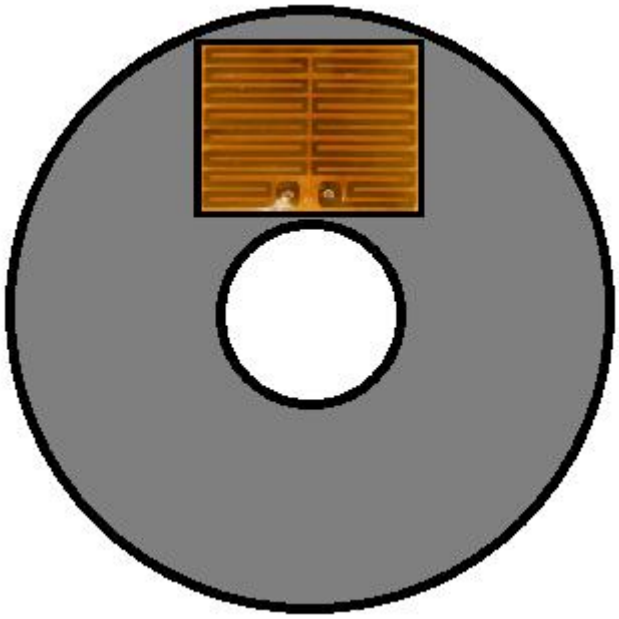

Figure 2: Location of the heating elements on the annulus base (colour online).

This arrangement effectively generates an "isolated ridge" of thermal topography, by analogy with Marshall and Read's (2018) Partial Barriers experiments. This arrangement also contrasts somewhat with Boubnov Golitsyn and Senatorsky's (1991) wavenumber-2 azimuthally-varying heating, which was generated by an azimuthal modulation of the temperature of the outer boundary that was held constant at all heights, rather than via an input heat flux imposed at the base. Boubnov, Golitsyn and Senatorsky note that, at its maximum, "the temperature contrast between continents and oceans is of the same order as the temperature difference between tropical and polar regions." In the present experiments, therefore, it was decided add the facility to generate an azimuthal thermal contrast of roughly 2 K via a patch of heating elements, so that the azimuthal heating contrast could be imposed on a similar scale to that of the radial heating during a typical experiment in which the radial temperature contrast $\Delta T = 2$ K (the weakest of the temperature differences used). This 2 K azimuthal thermal contrast is somewhat arbitrary, but convenient for creating a situation in which local and radial heating

could be made to be equivalent in strength. This chosen value also means that increasing the radial temperature difference for the experiments will in turn change the amount of relative heating if the azimuthal heating is held fixed. When the temperature difference between the walls of the annulus is larger than 2 K, then the azimuthal heating is weaker than the radial heating, permitting observation of the impacts this has on the flow structure. The calculation for achieving 2 K of heating is found by rearranging the definition of the Nusselt Number in an annulus, from Hide and Mason (1975), in terms of total heat transport, as follows:

$$H = \frac{2\pi Nud\kappa\rho c(T_b - T_a)}{\ln(b/a)}, \tag{3}$$

where H is the total heating power, Nu is the Nusselt Number, defined as the ratio of the total heat transfer to the conductive heat transfer in the fluid, D is the annulus depth, κ is the thermal diffusivity of the working fluid, ρ is the density of the fluid, c is the specific heat capacity of the fluid, and T_a and T_b are the temperatures at the inner and outer walls, respectively. This can be simplified by using the identity:

$$\kappa\rho c = \lambda, \tag{4}$$

where λ is the thermal conductivity of the fluid. Substituting this into (3) gives:

$$H = \frac{2\pi Nud\lambda(T_b - T_a)}{\ln(b/a)}. \tag{5}$$

Assuming a value of order 10 for the Nusselt Number (judging from previous experiments such as Hide and Mason 1975 and Read 2003, for example), and using a value of 0.5 $WK^{-1}m^{-1}$ for the thermal conductivity of a 17.5 / 72.5% glycerol/water mixture, from Glycerine Producers' Association (1963), gives a heating power of 15 W for the equivalent of 2 K of zonal temperature difference. As the 2 K temperature difference was chosen somewhat arbitrarily to be similar in scale to the minimum temperature difference between the walls of the annulus, the exact amount of heating provided is of less importance than its relative value. Since direct temperature measurements of the fluid nearby the heating

source were not employed, as the probes were found to have a non-negligible effect on the flow structure, the current study therefore uses 15 W of heating as the uniform parameter between all experiments. Preliminary testing showed that this amount of azimuthal heat input was able to create this azimuthally-varying heating profile, producing a discernible effect qualitatively equivalent to the mechanical isolated ridge of Marshall and Read (2018).

The results gathered were taken over a substantial range of parameter space, covering rotation rates from 0.4 rad s^{-1} to 2 rad s^{-1}, at intervals of 0.2 $rads^{-1}$, and temperature differences from 2 K to 7 K, at intervals of 1 K. Each individual realisation was observed and recorded for 1100s, starting at 3600s after spin up to allow the flow to equilibrate.

3. Flow regimes and phenomena

This section will focus on comparisons of flow structure between thermal topography and a single isolated ridge, as a way of studying the comparative effects of thermal topography on the structure and behaviour of a baroclinic flow. The experiments were designed in such a manner as to allow immediate comparison of the results gathered to those of Marshall and Read (2018) with a mechanical topographic barrier or ridge - by working over the same range of parameter space, and using a similar shape of base in azimuth (i.e. the heating elements on the flat base occupied roughly the same azimuthal area as the Marshall and Read's isolated ridge). Any differences between the results gathered should therefore be due to the influx of heating. As discussed above, this study is motivated by questions concerning the magnitude of influence and role thermal topography plays in the circulation patterns of atmospheres and oceans, as well as currently unresolved questions about the existence of multiple equilibria in geophysical contexts.

3.1. Results and analysis

The locations of various types of flow regime encountered in the experiments are shown in the following section in the form of a two-parameter regime diagram in figure 3. This regime diagram was compiled by identifying the dominant flow structure at each investigated point in parameter space. Both real-time streakline images and horizontal vector velocity field maps created by CIV were used to identify the principal flow regimes.

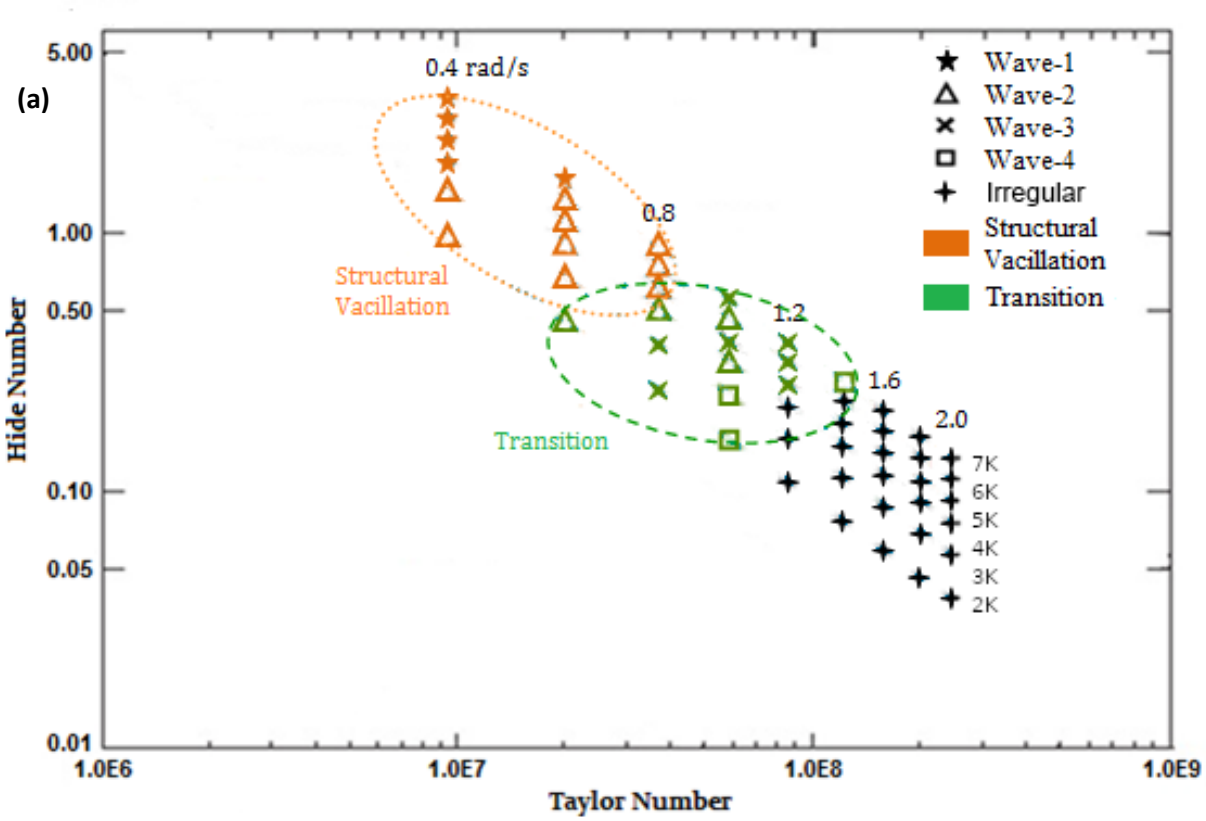

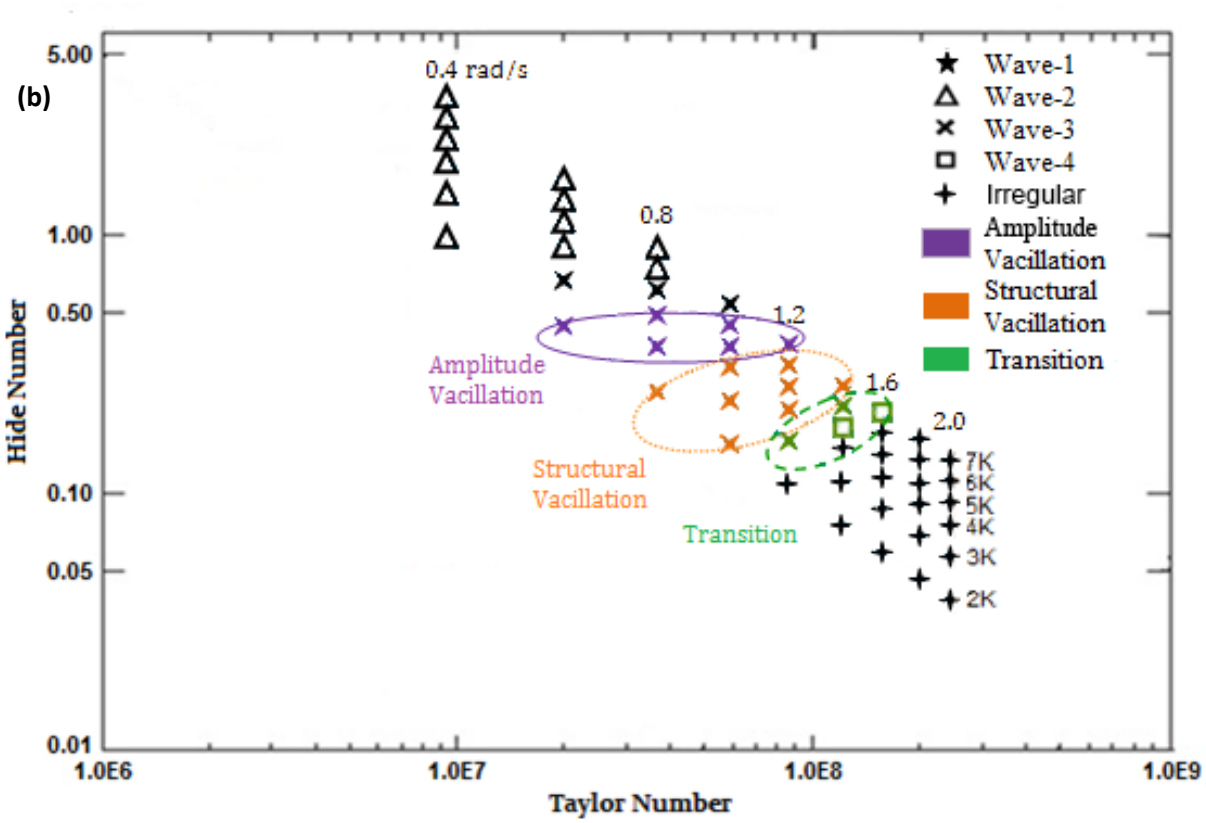

Figure 3: Regime diagram with locations and dominant flow characteristics of the results for: a.) Thermal Topography experiments, b.) Partial Barrier Experiments (adapted from Marshall and Read 2018, colour online).

As was the case for the mechanical topography study in Marshall and Read (2018), reproduced here as figure 3(b), the results of thermal topography experiments shown in the regime diagram in figure 3(a) fall into either of two major sections: an 'interference' region, occurring at larger Hide Numbers, where the impact of the stationary wave disturbance forced by the topography is strongly observable throughout the flow; and an 'irregular' region, at lower Hide Numbers, where the flow is erratic in time and space. Within the 'interference' regime, baroclinic waves can be observed, though the circulation never becomes a purely axisymmetric flow (almost certainly due to the asymmetrical topography), but instead always contains a drifting wave structure, transitioning from wavenumber-1 to wavenumber-2 to wavenumber-3, and with occasional transitions to wavenumber-4, as the rotation rate increases. The 'interference' flows show evidence of structural vacillation, whereby the dominant flow structure of the fluid varies over time, but with a consistent and regular pattern, in this case due to interference from the topography. Amplitude vacillation, wherein the wavenumber of the flow does not change but the scale

of the eddies vary, was not observed in any of the current experiments. Conversely, points within the dashed (green online) Transition region of figure 3(a) exhibit a greatly increased number of transitions between wavenumbers over time. In these flows, which lie near the 'irregular' region, a given dominant wavenumber is only foremost for part of the time, with other wavenumbers irregularly dominating the structure. This is especially common between wavenumber-3 and wavenumber-4, as those are the wavenumbers most often encountered before erratic behaviour takes over. Typically, the transitions are between adjacent wavenumbers, so that wavenumber-2 may transition to wavenumber-1 or wavenumber-3 and wavenumber-3 may transition to wavenumber-2 or wavenumber-4. This could suggest a low-dimensional wavenumber competition via wave-zonal flow nonlinear interactions (see e.g. Read *et al.* 1992). Dominant wavenumbers higher than four were not found, though higher non-dominant wavenumbers were temporarily noted.

Compared with Marshall and Read's (2018) Partial Barriers experiment, the regime diagram of the present experiments with thermal topography lacks a region without vacillation, and exhibits a wider range of possible transient (i.e. non-dominant) wavenumber components during transitions for the 'interference' regime, including wavenumber-1, wavenumber-4 and even, rarely, wavenumber-5. The major difference between the two cases is that the transition to the 'irregular' regime occurs both more gradually, leading in turn to larger vacillation and transition regions, and at a higher Hide Number. This could possibly be due to the thermal topography at the lower boundary effectively reducing the static stability of the fluid flow. As such, many of the flows near the transition between regimes exhibit strong vacillation and themselves transition frequently between wavenumbers.

Surprisingly, figure 3(a) shows no real evolution of the flow structure as the temperature difference is increased, beyond that which is also observed in Marshall and Read (2018) for the mechanical case. At both $\Delta T = 2$ K, where the radial and azimuthal thermal contrasts are equal, and at $\Delta T = 7$ K, where the radial heating is strongly dominant, the flow shows a steady progression from small wavenumbers to higher ones, with increasing tendency towards vacillation as the rotation rate increases. Hence, the effects of the azimuthal heating seem to be independent of the strength of radial heating, at least within the range explored here.

To examine the 'interference' and 'irregular' regimes in greater detail, one representative example from each region will be explored in terms of the evolution of the flow structure over time. For the 'interference' region the location in parameter space of this example will be $\Omega = 1.0$ rads^{-1}, $\Delta T = 4$ K, $\mathcal{T} = 5.680 \times 10^8$, and $\Theta_T = 0.316$. Likewise, for the 'irregular' region the example location will be $\Omega = 1.6$ rads^{-1}, $\Delta T = 4$ K, $\mathcal{T} = 1.454 \times 10^8$, and $\Theta_T = 0.124$.

3.1.1. Time-dependent 'interference' flow structure

In addition to the above, it was noted that the drifting waves are modified as they encounter and cross the topography, creating temporary flow structures at all levels of the annulus in the vertical direction. For the Thermal Topography experiments, whilst the same interference effects are observable at high Θ_T as in the experiments with mechanical topography (see figure 5 of Marshall and Read 2018), many of the flows near the transition between regimes exhibit strong vacillation and themselves transition frequently between wavenumbers, as mentioned previously. To illustrate this effect, an example of the time variations of the flow structure from this transition region is presented in figure 4.

To demonstrate the main aspects of the 'interference' regime near the 'irregular' regime in the context of the thermal forcing, the location of the heating elements has been added to figure 4(a). The flow in (a) starts off as a clockwise drifting wavenumber-2, experiencing heavy structural vacillation presumably due to its proximity to the irregular/chaotic transition, and is therefore more irregular and disordered than its wavenumber-3 equivalent from Marshall and Read's (2018) Partial Barriers experiment (figure 5(a) in that paper). As one of the cyclonic eddies approaches the thermal topography in (b), it begins to decay, and a new eddy begins to grow just downstream of the heating elements. Notably, at this point, the circulation becomes extremely asymmetrical, with a very large anticyclonic eddy upstream of the topography (anticlockwise), and barely any eddy activity downstream of the topography. This effect is temporary, since it disappears by (c), wherein the flow returns to being a wavenumber-2 structure, rather than a skewed wavenumber-1, as in Marshall and Read's Partial

Barriers study. These processes are again likely due to the influences of the nearby ‘irregular’ regime. By (d), further vacillation has set in, causing the circulation to transition to an irregular wavenumber-4 structure. This image is noteworthy in particular, as it strongly resembles the blocked state found by Weeks *et al.* (1997). This form is again temporary, with (e) showing a structure that appears to be a superposition of wavenumber-1 and wavenumber-2. As the pattern drifts further still, in (f), the flow again becomes dominated by a wavenumber-2. The example given in figure 4 shows the flow at mid-depth, but similar behavior can be found at all levels including near the bottom, as the replacement of the isolated ridge with the thermal topography means the lower depths of the annulus are no longer physically blocked. This will be discussed further in the next section. At lower rotation rates, these transitions are less common, and lower wavenumbers are seen to be dominant.

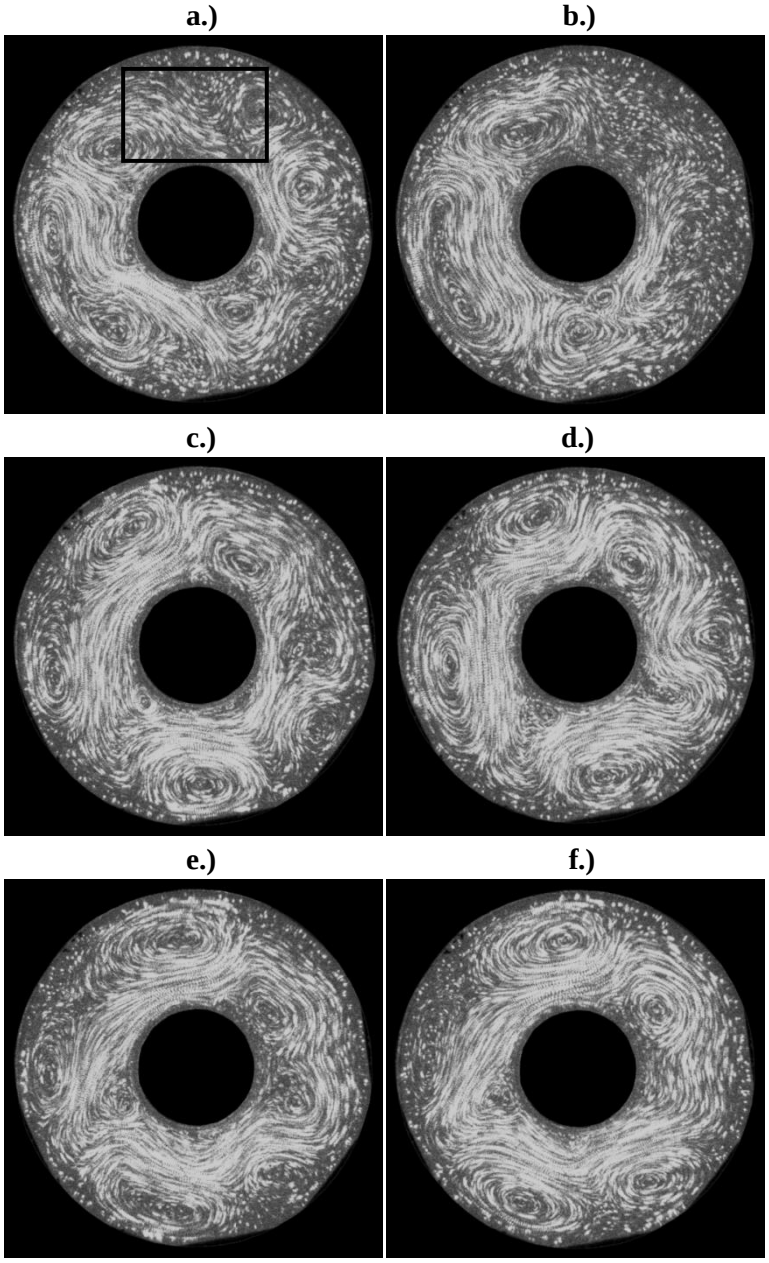

Figure 4: Streakline series for Thermal Topography Experiments Level 3 (mid-depth), $\Omega = 1.0$ rads^{-1}, $\Delta T = 4$K, $\mathcal{T} = 5.680 \times 10^8$, $\Theta_T = 0.316$, a.) t $= 3700$s, b.) $t = 3760$s, c.) $t = 3820$s, d.) $t = 3880$s, e.) $t = 3940$s, f.) $t = 4000$s.

To illustrate the 'interference' regime flow structures over a longer timescale than the image sequence above, figure 5 shows an azimuth-time Hovmoller diagram of the radial velocity for every point on a complete azimuthal circle at mid-radius over the entire 1100s run. Unfortunately, as the example location in parameter space used for figure 4 was so close to the 'irregular' regime, a Hovmoller diagram produced at the same location was found to be cluttered and with difficult to observe

key features. Due to this, figure 5 is instead generated from a scan at a different location, further into the 'interference' region. Azimuthal position is given in degrees (where positive is anticlockwise), and within with the centre of the heating elements is located at about 100°.

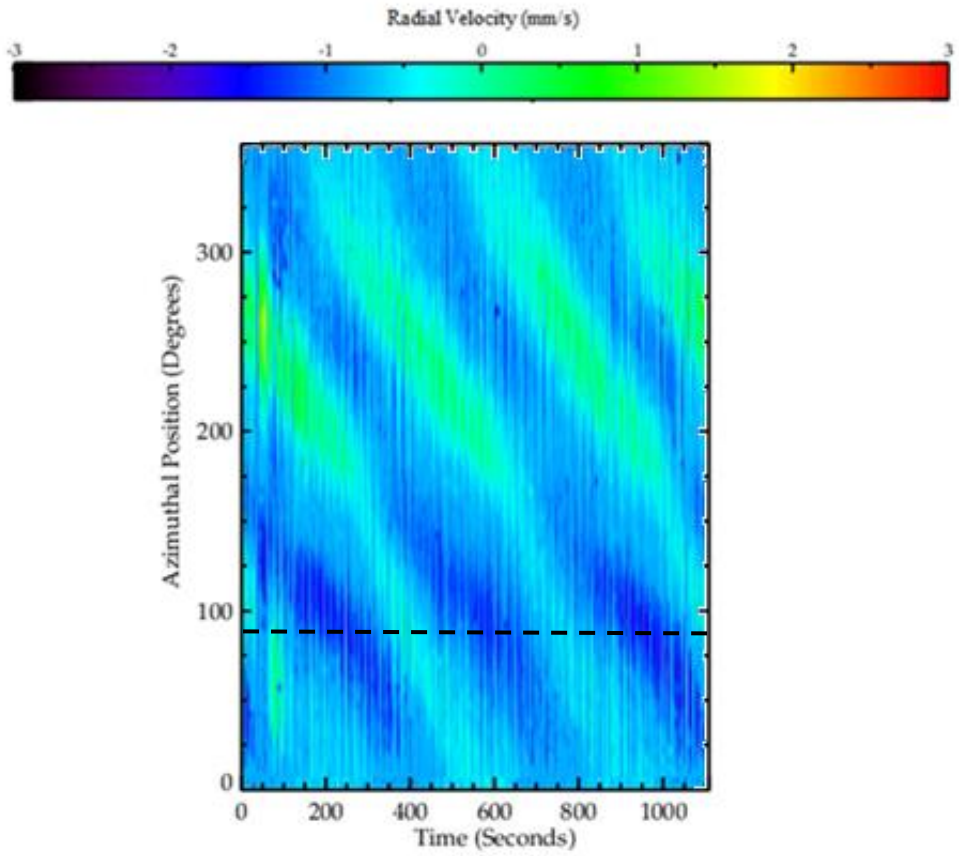

Figure 5: Radial velocity as a function of time and azimuthal position at mid-radius for Level 3 (mid-depth), $\Omega = 0.4$ rads^{-1}, $\Delta T = 4$K, $\mathcal{T} = 9.088 \times 10^6$, $\Theta_T = 1.976$. The time origin refers to beginning of recording, 1 hour after spin up. The black dashed line denotes the centre of the heating element (colour online).

Figure 5 shows the continuously clockwise drifting wavenumber-2 structure of the flow throughout this example of the 'interference' region of parameter space, becoming more negative in azimuthal position over time. The impact upon the wave as it encounters the topography is also highlighted, which begins at around an azimuthal position of 175°. At this point, the drifting wave can be observed to reduce greatly in strength, becoming difficult to discern from the flow between waves. This is equivalent to the apparent visual disappearance of the wave as it encounters the topographic

peak as shown in figure 4. The phase of the drifting wave is also notably modified as it crosses the topographic peak. In addition, figure 5 suggests that the same wave that disappears when crossing the topography is indeed the same wave that reappears once the flow has moved on, due to the unbroken peak or trough connecting the drifting flow on either side of the topography. The zonal mean value of radial velocity in the area near the heating elements is different from that in the area opposite the elements, suggesting that there exists a large-scale circulation between the two regions, due to the thermal topography's localised heating. Compared to the experiments with mechanical topography in Marshall and Read's (2018) figure 6, both cases show very similar results, aside from the drifting waves with thermal topography travelling with a lower drift rate than those with partial barriers, likely due to lower rotation rate in the former case. This in turn causes the drifting wave with thermal topography to take a much greater time and distance to regain its original strength after reappearing, only doing so at around an azimuthal position of 250°.

3.1.2. Time-dependent 'irregular' flow structure

In Marshall and Read's (2018) Partial Barrier experiments, an 'irregular' region appeared abruptly in the mapped parameter space, and at much lower rotation rates and temperature differences than would be expected for such an erratic flow without the presence of asymmetrical bottom topography or heating. Some of the unusual properties of the regime were illustrated in that paper's figure 4, giving a brief example of the flow structure. An 'irregular' regime was also found to occur in a similar way in the Thermal Topography experiments, with fine-scale features, such as small, asymmetrically-placed eddies downstream of the heating elements and a permanent large eddy or a jet just upstream of the elements. However, as mentioned previously, the 'irregular' regime appears far less abruptly in the present experiments as the rotation rate is increased, with a noticeable but slow transition from one regime to the other.

To illustrate the 'irregular' regime flow structure over a long timescale figure 6 shows a Hovmoller plot of the radial velocity for every point on a complete azimuthal circle at mid-radius, for a typical flow in the 'irregular' regime from the Thermal Topography experiments. Once again, azimuthal position is given in degrees, where positive is anticlockwise, and within which the centre of the heating elements is located at about 100°.

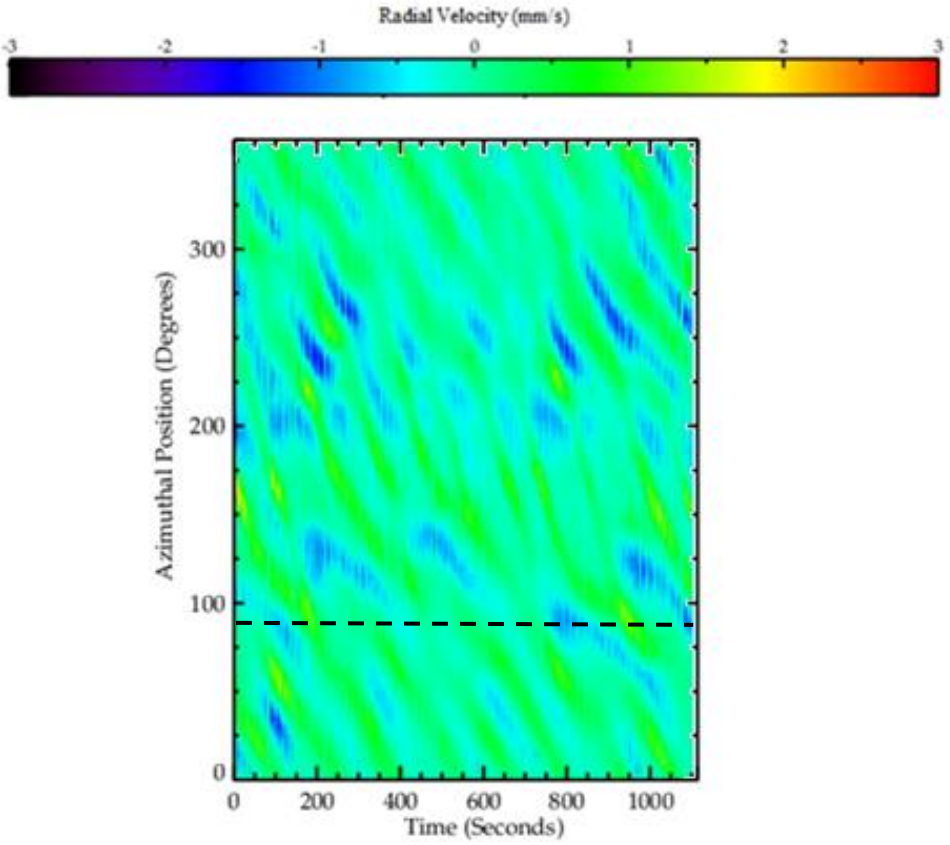

Figure 6: Radial velocity over time against azimuthal position at mid-radius for Level 3 (mid-depth) at $\Omega = 1.6$ rads^{-1}, $\Delta T = 4$K, $\mathcal{T} = 1.454 \times 10^8$, $\Theta_T = 0.124$. The time origin refers to beginning of recording, 1 hour after spin up. The black dashed line denotes the centre of the heating element (colour online).

Much like for the Partial Barriers experiment in figure 8 of Marshall and Read (2018), figure 6 shows a far more erratic flow structure throughout the entire run than in the 'interference' regime case in figure 5, but also shows that the flow is not purely random in nature. In addition, some clockwise drifting wave structures representing several different wavenumber components can be observed. These different wavenumber components have varying drifting rates, and often overlap each other,

contributing to the erratic nature of the flow. Interestingly, however, the impact of the thermal topography seems to be greatly reduced compared both to the mechanical topographic experiments and to the 'interference' regime, with the strongly erratic flow structure near the heating elements appearing very similar to the structure far away from them.

3.2. Time-averaged flow structure

Taking a time-average of the flow structure over the period of the drifting waves (taken from figure 4 to be about 400s), has the effect of removing the drifting wave elements and leaving only the stationary components. To illustrate this, figure 7 gives an example of time-averaged flow for the 'interference' regime using a kinetic energy map for the parameters given in figure 5.

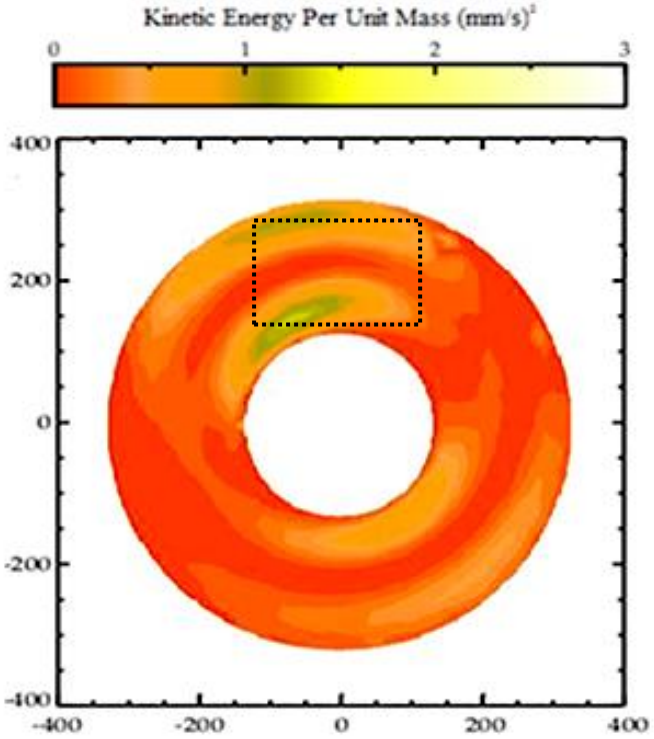

Figure 7: Kinetic energy averaged over 400s for Level 3 (mid-depth) for $\Omega = 0.4$ rads^{-1}, $\Delta T = 4$K, $\mathcal{T} = 9.088 \times 10^6$, $\Theta_T = 1.976$. The black dotted box denotes the location of the heating element (colour online).

As figure 7 illustrates, with the drifting wave components removed by the time-averaging, a great deal of the flow structure is removed. By combining the averaged velocity components into a kinetic energy map to illustrate the total flow structure, only a single notable persistent jet remains, forming a stationary vortex directly above the bottom topography. This is evidence for a pressure drop as the flow crosses the heating elements (since the radial and azimuthal velocities show that the relative vorticity is cyclonic), and also highlights the relative lack of stationary wave elements. In addition, the stationary "imaginary cylinder" occurring in the flow directly above the actual topography suggests an analogy with a Taylor column (see Taylor 1923). Furthermore, figure 7 shows that Taylor columns can occur even without mechanical topography, as an "imaginary cylinder" that is created purely from azimuthally-varying thermal forcing. This feature will be discussed further in the analysis of the vertical structure of the fluid flow in the annulus (section 3.5). Whilst the results of Marshall and Read's (2018) Partial Barrier experiments (figure 9 in that paper) and the present Thermal Topography experiments are very similar, for the latter the jet is stronger and more circular in nature, creating a full persistent gyre over the heating elements. Furthermore, the thermal topography also appears to produce aspects of a wavenumber-2 stationary component, with a minor secondary eddy opposite the heating elements. This bears similarity with the atmospheric circulation that is believed to occur in tidally-locked exoplanets, wherein a strong vortex is found to occur on the dayside, and a weaker vortex occurring on the nightside (as discussed, e.g., by Cho 2008). It would therefore seem likely that thermal topography in a baroclinic annulus has the ability to replicate at least some of a tidally-locked atmosphere.

Similarly, figure 8 shows a time-average of the flow structure over the period of the drifting waves for the 'irregular' regime using a kinetic energy map at the parameters given in figure 6. Figure 8 demonstrates that the 'irregular' region has a very similar time-averaged structure to the 'interference' region, with weak stationary elements except for a single notable persistent jet occurring directly above the bottom topography. The jet and corresponding pressure drop as the flow crosses the topographic peak are significantly larger in amplitude for the 'irregular' regime, as was the case for mechanical topography (see figure 10 in Marshall and Read 2018). Unlike the experiments with mechanical topography, however, the 'irregular' region with thermal topography appears to have a reduction in

wave activity at locations away from the heating elements when the Taylor number is increased. Unlike the 'interference' regime in figure 7, this weak wave activity appears to have a wavenumber-3 stationary component, rather than wavenumber-2.

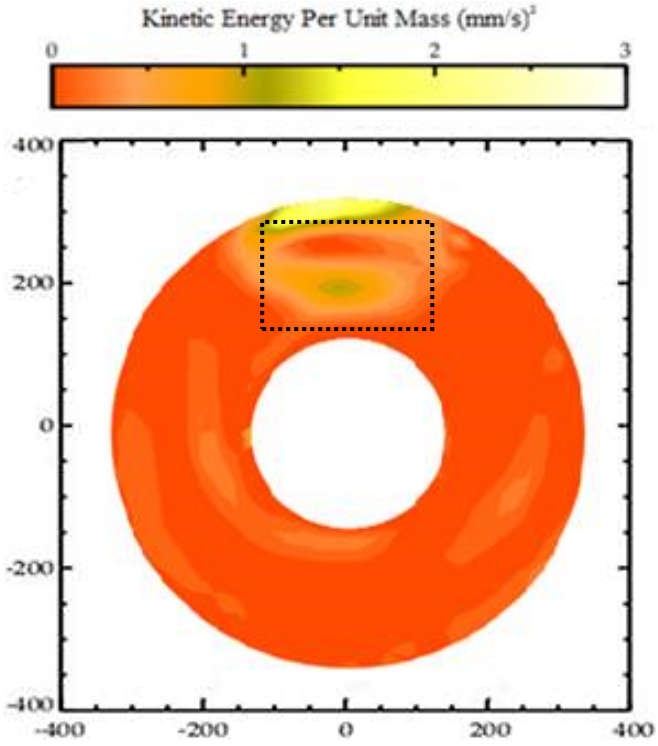

Figure 8: Kinetic energy averaged over 400s for Level 3 (mid-depth) at $\Omega = 1.6$ rads^{-1}, $\Delta T = 4$K, $\mathcal{T} = 1.454 \times 10^8$, $\Theta_T = 0.124$. The black dotted box denotes the location of the heating element (colour online).

3.3. Bottom flow structure

One of the major differences between mechanical topography and thermal topography is that in the former case, at the lowest vertical level observed, the horizontal flow is physically blocked by the topographic peak of the base. The flow is therefore forced to create an azimuthally-trapped structure (though fluid may be driven upwards over the ridge), different to that found at the higher unobstructed levels. Marshall and Read's (2018) figure 11 gives an example of this trapped flow, at a point in parameter space close to the boundary between the 'interference' and 'irregular' regimes. In contrast, at the lowest level observed in the present Thermal Topography experiments the flow is uninterrupted,

as illustrated in figure 9 for a similar point in parameter space between the 'interference' and 'irregular' regimes.

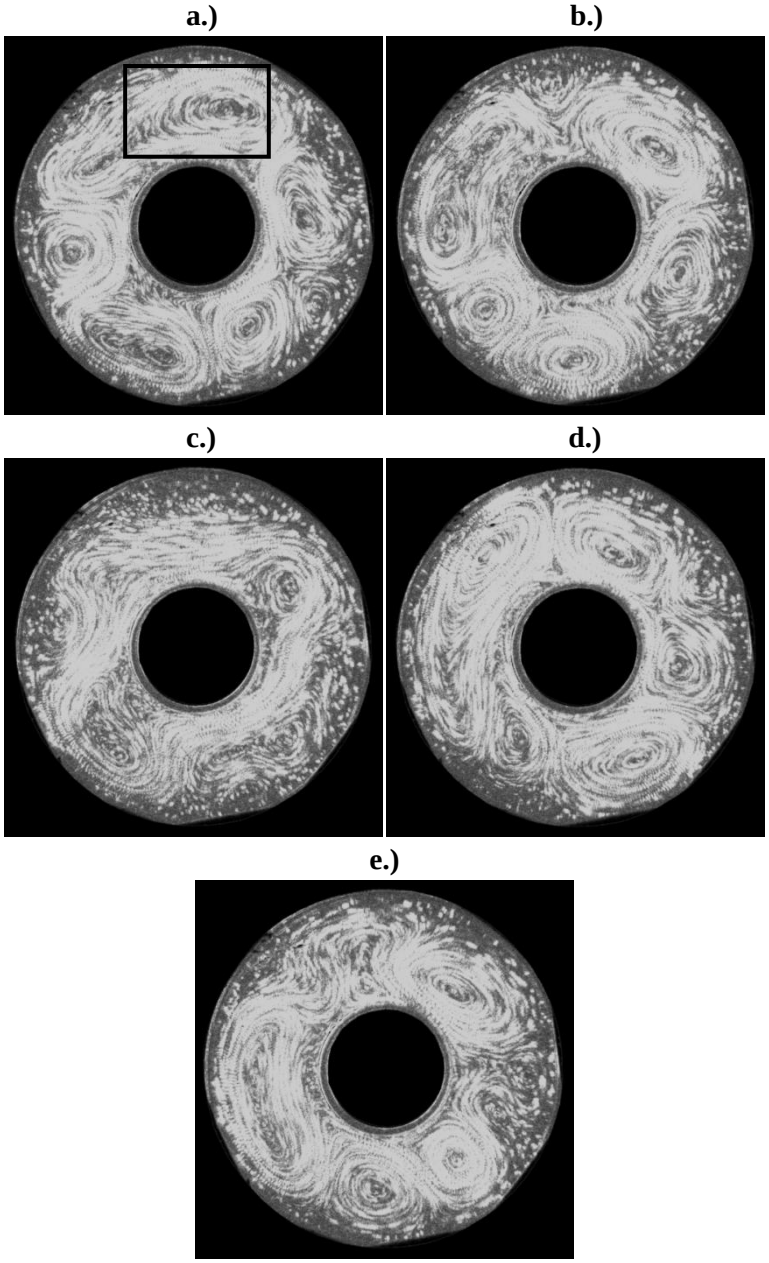

Figure 9: Streakline Series at Level 5 (bottom), $\Omega = 1.0$ rads^{-1}, $\Delta T = 4$K, $\mathcal{T} = 5.680 \times 10^8$, $\Theta_T = 0.316$, a.) $t = 4100$s, b.) $t = 4180$s, c.) $t = 4260$s, d.) $t = 4340$s, e.) $t = 4420$s.

Figure 9 shows the main aspects of the low-level flow over the thermal topography, with an indication of where the heating elements lie added to (a). Without the physical barrier to the flow's progression, the circulation no longer creates a persistent azimuthally-trapped wave upstream (anticlockwise) of the peak, nor does it give rise to the smaller-scale downstream eddies, as in Marshall

and Read (2018). Instead the flow resembles more the image sequence in figure 4, with irregular drifting wavenumber-2 components, seen most clearly in (c), but with notable vacillations and transitions in flow structure. This suggests that the flow is more uniform in the vertical direction than in Marshall and Read's Partial Barriers experiments, as there is no separation between blocked and unblocked flow. However, the structure at the bottom of the annulus does appear to be undergoing stronger chaotic variability than at higher levels. This is likely to be caused by the proximity to the base's heat source, injecting additional energy into the flow and reducing the local static stability. Whilst the above just gives a single example taken from one point in parameter space, the observation that flow at the bottom level was mostly similar to that seen at the higher levels (except with possible increased tendency for vacillations and wavenumber fluctuations) is typical of the behavior encountered throughout this investigation.

3.4. Time variations in amplitude and phase

To allow further understanding of the observed oscillations, an azimuthal Fourier analysis of the wavenumber structure in terms of their amplitudes and phases was carried out for every time step. Combining these analyses allows the evolution of the flow over time to be observed. After the zonal background mean flow was removed, azimuthal velocity components were calculated at a quarter of the radial distance between the inner wall and the outer wall (closer to the inner wall) and radial velocity components were calculated at mid-radius. In this way, nodes in the radial direction could be avoided.

3.4.1. 'Interference' regime Fourier analysis

Figure 10 shows an example of the time variations of the amplitude of the first four wavenumbers, for typical flows in the 'interference' regime, far away from the boundary with the 'irregular' regime, for the same parameters as used in figure 5.

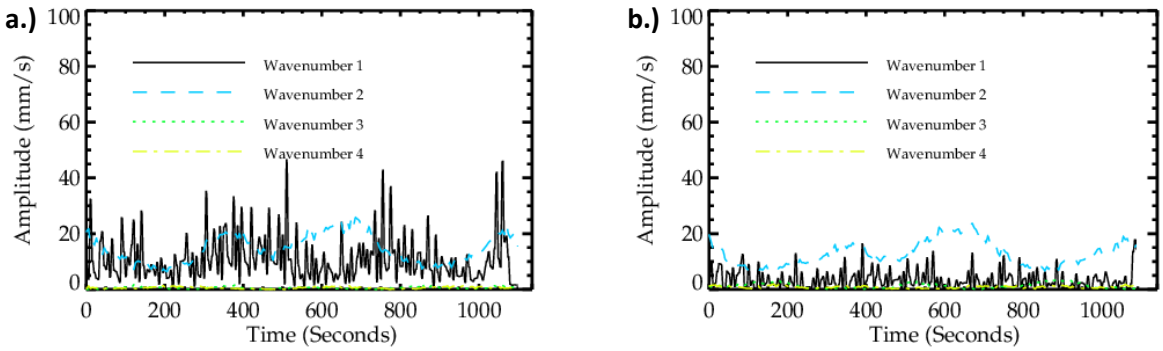

Figure 10: Velocity amplitude for wavenumbers 1-4 at Level 3 (mid-depth) at $\Omega = 0.4$ rads^{-1}, $\Delta T = 4$K, $\mathcal{T} = 9.088 \times 10^6$, $\Theta_T = 1.976$; a.) azimuthal velocity, b.) radial velocity. The time origin refers to beginning of recording, 1 hour after spin up (colour online).

As can be seen in figure 10, the flow in the 'interference' region is primarily comprised of wavenumber-1 and wavenumber-2 components, with the wavenumber-2 dominant in the radial case, and both roughly equal in the azimuthal case. It can be noted that the amplitudes of the latter are higher than the amplitudes of the former, whereas, in Marshall and Read's (2018) Partial Barriers study it was the opposite (see that paper's figure 12). The strong and noisy wavenumber-1 component (which is found to be dominant at other radius locations) was also not observed in any of Marshall and Read's experiments with mechanical topography, suggesting that this feature and its fluctuations are likely associated with thermal forcing from the wavenumber-1 shaped topography. Despite this, the rest of the flow structure is similar. In particular, the peaks of the wavenumber-2 component match the troughs of the wavenumber-1 component, although to a lesser extent than in Marshall and Read's (2018) Partial Barriers experiment case, presumably due to the weaker forcing conditions. As in Marshall and Read's investigation, this is caused by eddies encountering the topography and transitioning between two sequential wavenumber structures, in this case wavenumber-1 and wavenumber-2, as shown in figure 4 for a case with wavenumber-2 and wavenumber-3.

By examining the phases over time of the first ten wavenumbers of the flow at the same parameters as in figure 10, most of the wave components were found to be steadily drifting. As the flow with thermal topography at this location in parameter space is dominated by wavenumber-1 and wavenumber-2 components, figure 11 shows the phases of these notable wavenumbers.

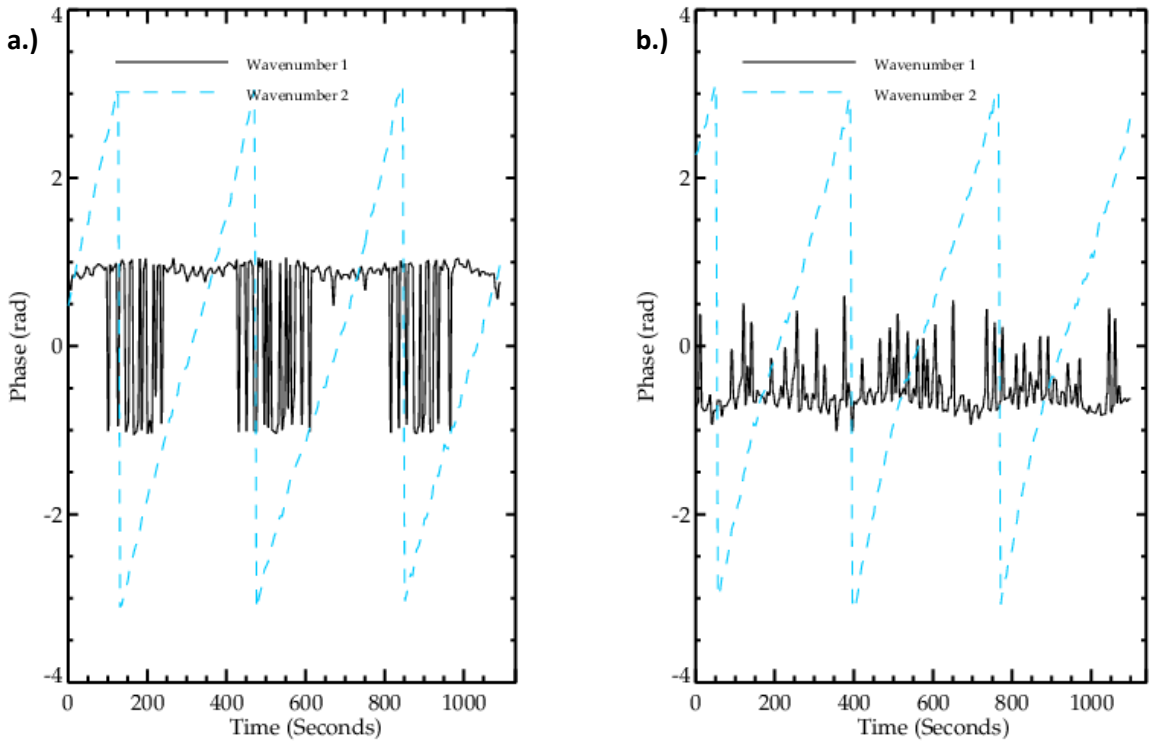

Figure 11: Velocity phase at Level 3 (mid-depth) at $\Omega = 0.4$ rads^{-1}, $\Delta T = 4$K, $\mathcal{T} = 9.088 \times 10^6$, $\Theta_T = 1.976$; a.) azimuthal velocity for wavenumber-1 and wavenumber-2, b.) radial velocity for wavenumber-1 and wavenumber-2. The time origin refers to beginning of recording, 1 hour after spin up (colour online).

Both (a) and (b) of figure 11 show that the wavenumber-2 component, like the other components not shown, is constantly drifting, but the wavenumber-1 component is stationary (quasi-stationary in the azimuthal case). This is of interest, as our studies of the flow near the bottom of the annulus in this case showed no azimuthally-trapped wave structure, so this stationary wavenumber-1 component must arise directly from the pattern of thermal forcing, and not in the arresting of a drifting structure. The 'interference' flow structure therefore appears to be mainly caused by interactions between the drifting waves and a locked stationary wavenumber-1 component. During periods where the two are out of phase, they constructively interfere, creating a wavenumber-2 flow. In periods where they are in phase, they destructively interfere, creating a wavenumber-1 flow. As a similar effect was noted in Marshall and Read's (2018) Partial Barriers experiments (see that paper's figure 13), it is suggested that these interactions arise regardless of whether the topography is mechanical or thermal in nature. On the other hand, the period of the oscillation does appear to change depending on topography.

The present thermal topography generates a period of roughly 400s for both the topographic interaction (see figure 4) and the phase interaction (figure 11), but for mechanical topography the period of both was about 200s.

For further investigation, figure 12 shows the variations of the radially-averaged kinetic energy of the first four azimuthal wavenumbers over time.

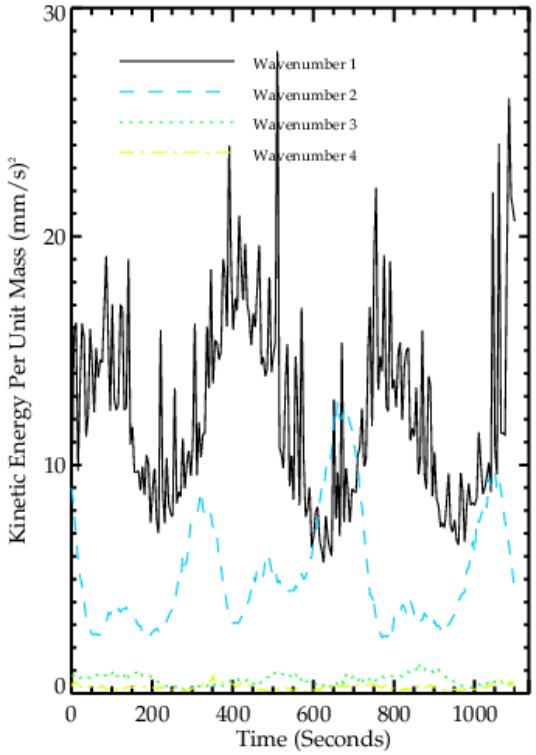

Figure 12: Radially-averaged kinetic energy for wavenumbers 1-4 at Level 3 (mid-depth) $\Omega = 0.4$ rads^{-1}, $\Delta T = 4$K, $\mathcal{T} = 9.088 \times 10^6$, $\Theta_T = 1.976$. The time origin refers to beginning of recording, 1 hour after spin up (colour online).

Figure 12 confirms what was just described, with the kinetic energy of the flow being transferred back and forth between the wavenumber-1 component (now dominant, suggesting variations in wavenumber composition over radial location) and the wavenumber-2 component, with the amplitude peaks of one wavenumber aligning with the troughs of the other. Indeed, the relationship between the two oscillations is even easier to discern in the graph of kinetic energy, especially in terms of the period of roughly 400s. Comparing this with the equivalent case for mechanical topography

(figure 14 in Marshall and Read 2018), the similarities appear to suggest that the same process of topographic interaction is occurring, regardless of whether the oscillation is forced by mechanical or thermal topography. In addition, the time variation of the wavenumber-2 kinetic energy component appears to contain a period-doubled oscillation, only found at this large Hide Number region in parameter space.

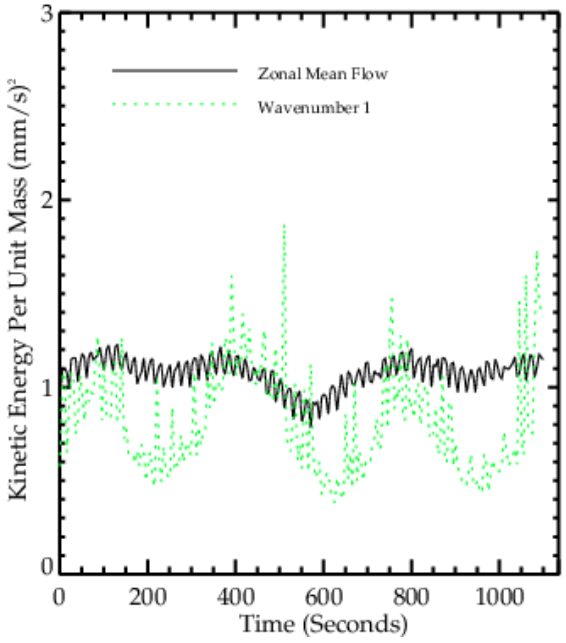

Figure 13: Radially-averaged kinetic energy of zonal mean flow (black) at Level 2 with wavenumber-1 total kinetic energy (green, not to scale) as comparison, at $\Omega = 0.4$ rads^{-1}, $\Delta T = 4$K, $\mathcal{T} = 9.088 \times 10^6$, $\Theta_T = 1.976$. The time origin refers to beginning of recording, 1 hour after spin up (colour online).

A contrast can be also made between the time variations of the kinetic energy of the dominant wavenumber-1 component and the kinetic energy of the zonal mean flow. At mid-depth, this zonal mean component is found to fluctuate in direction from positive to negative and vice versa, suggested to be due to being acted upon by both the topographically-forced stationary waves from the bottom that appear to dictate a 400s transitional oscillation and the free baroclinic waves from the top and middle of the tank. Hence, figure 13 shows the variation over time of the kinetic energy of the zonal mean from the same points in parameter space as in figure 12, but at the higher Level 2. A superposition of the wavenumber-1 kinetic energy time-series is also provided for comparison.

Figure 13 shows that the kinetic energy of the zonal mean flow oscillates roughly in quadrature with the kinetic energy of the dominant mode, with the zonal mean kinetic energy peaks occurring where the wavenumber-3 kinetic energy for mechanical or wavenumber-1 kinetic energy for thermal is changing most rapidly, and vice versa. As for mechanical topography (see figure 15 in Marshall and Read 2018) this is consistent with strong nonlinear wave-zonal flow interactions and an exchange of energy between the waves and the mean zonal flow. However, the correlation in the case with heating elements is much weaker than the case with the isolated ridge, suggesting that the nonlinear wave-zonal flow interactions occurring are of less significance to the overall flow structure, compared to wave-wave interactions for example, for thermal topography than for mechanical topography. In addition, the Thermal Topography experiments also have a higher frequency component in the zonal mean flow kinetic energy, with a period of around 30s.

3.4.2. 'Irregular' regime Fourier analysis

For contrast with the 'interference' regime, figure 14 gives the time variations of the amplitude of selected wavenumbers of typical flows in the 'irregular' regime, fairly distant from the region boundary, for the parameters used in figure 6.

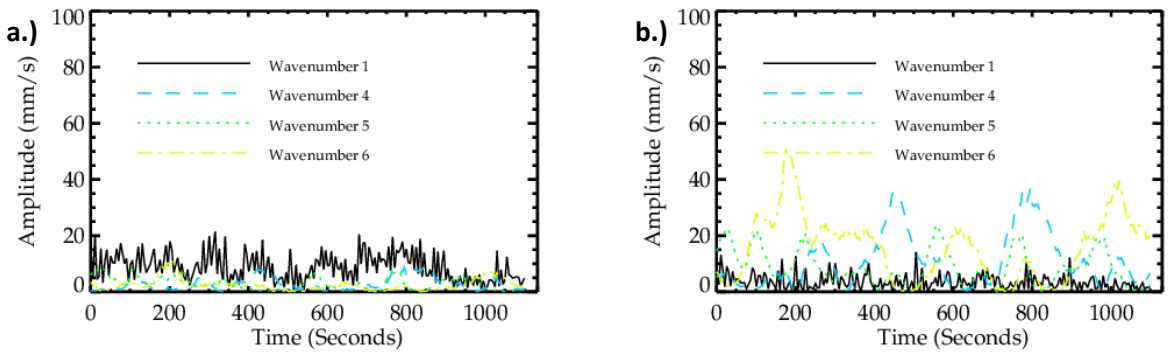

Figure 14: Velocity amplitude for selected wavenumbers for Level 3 (mid-depth) at $\Omega = 1.6$ rads^{-1}, $\Delta T = 4$K, $\mathcal{T} = 1.454 \times 10^8$, $\Theta_T = 0.124$; a.) azimuthal velocity, b.) radial velocity. The time origin refers to beginning of recording, 1 hour after spin up (colour online).

From figure 14, it can be determined where the ‘irregular’ regime originates. It can be noted that the previously dominant wavenumber-1 component is no longer the largest in amplitude. The azimuthal profile is now dominated for most of the time by an irregularly-varying wavenumber-1, and the radial velocity profile is dominated by much higher wavenumbers, chiefly wavenumbers 4, 5 and 6. These high wavenumber radial velocity amplitudes are also now much larger than the azimuthal amplitudes, which is also consistent with the irregularly-spaced small eddies and other fine-scale features found in the ‘irregular’ regime. If the Hide Number is increased, these radial components can be seen to increase steadily in amplitude as well.

By examining the phases over time of the first ten wavenumbers, most of the wave components were found to be steadily drifting, with the exception of wavenumber-1. As the ‘irregular’ regime flow is dominated by wavenumber-4, wavenumber-5 and wavenumber-6 components in radial velocity, figure 15 shows the phase of these notable wavenumbers, as well as the wavenumber-1 component, for the same flow case as in figure 14.

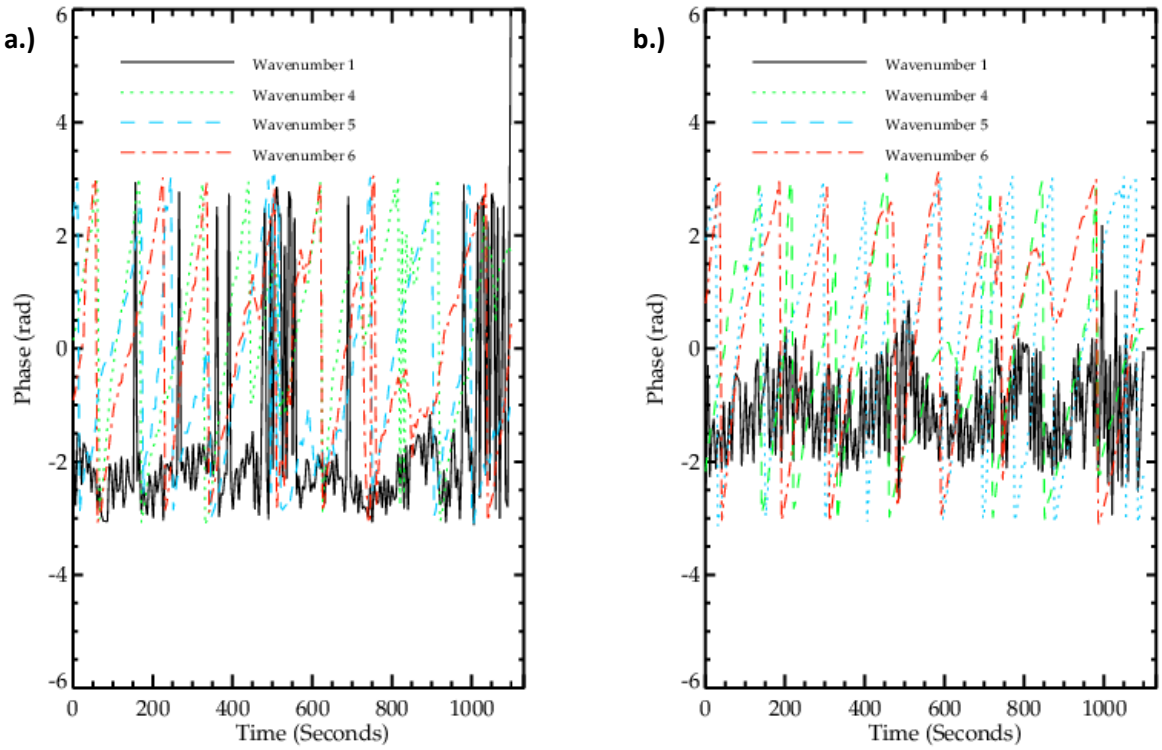

Figure 15: Wavenumber-1 phase (black) against wavenumber-4 phase (blue), wavenumber-5 phase (green) and wavenumber-6 phase (red), for Level 3 (mid-depth), $\Omega = 1.6$ rads^{-1}, $\Delta T = 4$K, $\mathcal{T} = 1.454 \times 10^8$, $\Theta_T = 0.124$, a.) azimuthal velocity, b.) radial velocity. The time origin refers to beginning of recording, 1 hour after spin up (colour online).

Figure 15 shows that the wavenumber-1 component is quasi-stationary, but the majority of the other components are still drifting. This stationary wavenumber-1 component is likely associated with the wavenumber-1 component of the thermal topography (though said topography is not wholly wavenumber-1 in structure). Marshall and Read's (2018) experiments with mechanical topography also found similar results, but the present study shows that the stationary wavenumber-1 component is independent of any azimuthally-trapped wave at the bottom level of the annulus, as it also occurs with the flat heating elements. Furthermore, by looking at the radial phase in (b), it can be noticed that wavenumber-4, wavenumber-5 and wavenumber-6 appear to show good evidence of phase synchronisation, despite the noise of the experiment, suggesting the activity of resonant wave-triads. As stated by Bretherton (1964), the two conditions for a resonant wave-triad are that the summation or difference of the vectors of the three wave modes, i.e. their wavenumbers, must be zero, and that the

drifting frequencies of the three wave modes must also be self-interacting and have a summation or difference that equals zero, as below:

$$k_m = k_{m'} + k_{m''} \tag{6}$$

and

$$\omega_m = \omega_{m'} + \omega_{m''}\,, \tag{7}$$

where m, m', and m'' are the three wave modes that make up the triad, k is the wavenumber of each mode, and ω is the modal drift frequency of each mode determined by the Rossby wave dispersion relation. Assuming that the wavenumber-1 topography plays a role in the interactions (which is judged to be reasonable due to the dominant stationary azimuthal velocity wavenumber-1 component), there are therefore two likely triads: one involving wavenumbers 4, 5 and the stationary, topographically anchored wavenumber-1 component, and another involving wavenumbers 5, 6 and the stationary, topographically anchored wavenumber-1 component. These wave-triads were also found to occur in Marshall and Read's (2018) experiments with mechanical topography.

Further to the above, as noted by Früh and Read (1997), integrating (7) with respect to time gives the following:

$$\varphi_m + \varphi_{m'} + \varphi_{m''} = \text{const.}\,, \tag{8}$$

where φ is the phase of each mode. The relative importance of a wave-triad to the dynamic evolution of the flow can be measured by how constant the summation or difference of the phases of the component wave modes remains over time. Hence, if the phases are 'unwrapped' then the behaviour of this phase difference over time between them can be observed, as in figure 16. This shows the differences between the wavenumber-5, wavenumber-4 and wavenumber-1 components and between the wavenumber-6, wavenumber-5 and wavenumber-1 components. These differences are both found by subtracting the unwrapped phase of the two middle wavenumber components (wavenumber-4 and wavenumber-5, respectively) from the sum of the unwrapped phase of the higher wavenumber

(wavenumber-5 and wavenumber-6, respectively) and wavenumber-1 components.

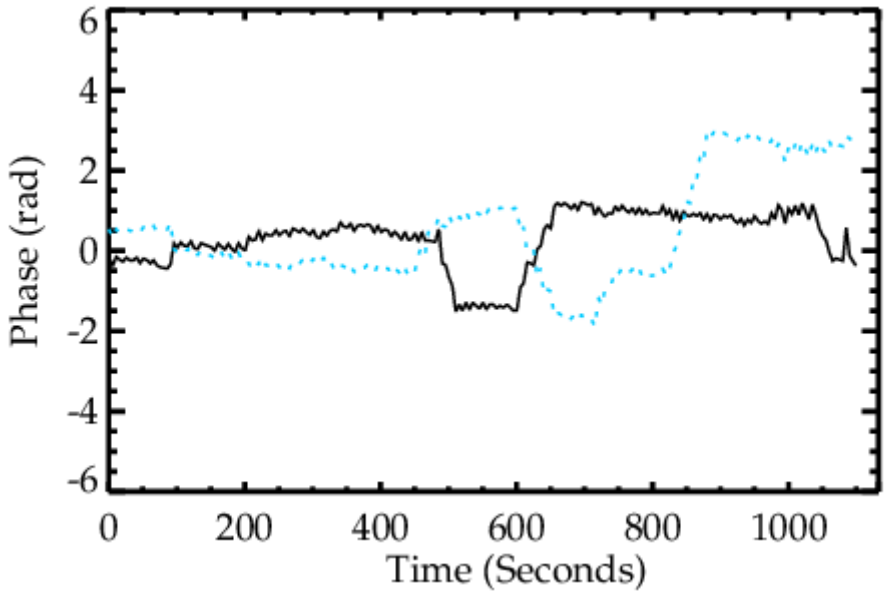

Figure 16: Unwrapped radial wavenumber-5, wavenumber-4 and wavenumber-1 phase difference ($\varphi_1 + \varphi_5 - \varphi_4$, solid black line) and unwrapped radial wavenumber-6, wavenumber-5 and wavenumber-1 phase difference ($\varphi_1 + \varphi_6 - \varphi_5$, dotted blue line) against time at $\Omega = 1.6$ rads^{-1}, $\Delta T = 4$K, $\mathcal{T} = 1.454 \times 10^8$, $\Theta_T = 0.124$. The time origin refers to beginning of recording, 1 hour after spin up (colour online).

In figure 16 the phase difference has long intervals of near-stationarity, giving evidence that these are indeed components of important, coherent wave-triads for the evolution of the flow, like those found in Marshall and Read's (2018) Partial Barriers experiments. There are also frequent phase-slips where the phase difference suddenly changes to a new constant value. In the case with mechanical topography (see figure 18 in Marshall and Read), these phase-slips had regular intervals equal to the time taken for one cycle of the topographic interaction, so it was suggested that these phase-slips may be associated with interactions with the topography as the flow drifted over the peak of the base. For the present thermal case, it can be observed that there is much less noise and there is a clearer structure than for mechanical topography. Although the phase-slips no longer appear to occur at particularly regular intervals, the longer intervals of near-stationarity, especially for the wave-triad comprised of wavenumbers 1, 4, and 5, appear to be of roughly 400s, which figure 4 gives as the time taken for one cycle of the topographic interaction.

Due to the similarities with Marshall and Read's (2018) Partial Barriers experiments, it appears that the 'irregular' regime, regardless of whether the topography used is mechanical or thermal in origin, involves the action of two resonant wave-triads: one between the stationary wavenumber-1 component, most likely forced by the topographic base, and the drifting wavenumber-4 and wavenumber-5 components; and the other again between the stationary wavenumber-1 component, but instead interacting with the drifting wavenumber-5 and wavenumber-6 components. In the literature, clusters of two triads that are connected by a common mode are referred to as "butterflies". Kartashova and L'vov (2007), for example, found evidence for three such "butterflies" playing a role in the dynamics of their numerical investigation into LFV in the Earth's atmosphere. Kartashova and L'vov put forward the idea that intraseasonal atmospheric oscillations could be described via "periodical energy exchange" within various planetary wave triads, including between the three "butterflies" that were able to exchange energy through their shared common modes. Once again, this gives evidence that the nonlinear interactions that cause the transition from the 'interference' regime to the 'irregular' regime have strong wave-wave components, with energy being transferred between the different wavenumber modes. In the current experiments, this "butterfly" is independent of any locally-blocked waves at the bottom of the annulus, occurring under any topography with a dominant wavenumber-1 structure.

In addition, for the 'irregular' regime, a contrast can again be made between the time variations of the kinetic energy of the dominant wave components and the kinetic energy of the zonal mean flow. Figure 17 shows the variation over time of the kinetic energy of the zonal mean from the same points in parameter space as in figure 14, but at the higher Level 2, and with a superposition of the total kinetic energy from the first ten wavenumbers (since there is no clear dominant wavenumber component) for comparison.

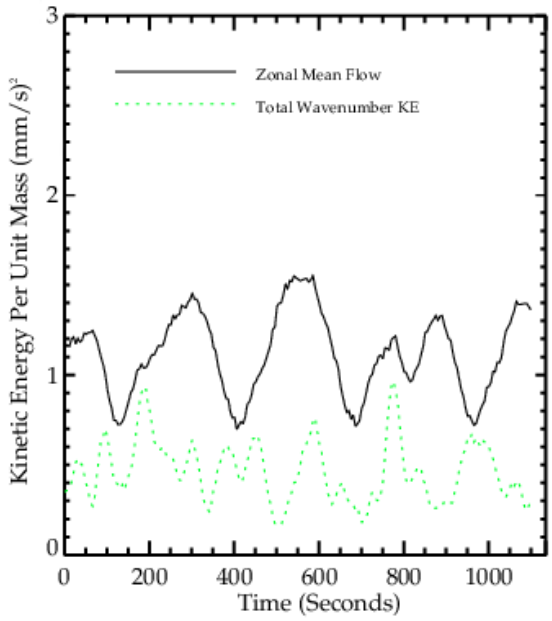

Figure 17: Radially-averaged kinetic energy of zonal mean flow (solid black line) with total kinetic energy (dotted green line, not to scale) as comparison, for Level 2 at $\Omega = 1.6$ rads^{-1}, $\Delta T = 4$K, $\mathcal{T} = 1.454 \times 10^8$, $\Theta_T = 0.124$. The time origin refers to beginning of recording, 1 hour after spin up (colour online).

Within the 'irregular' region, figure 17 shows that there is a much less pronounced correlation between the activity of the dominant component and the mean flow, as compared to the 'interaction' region. In Marshall and Read's (2018) experiments with mechanical topography some weak oscillating in quadrature was observed (see figure 19 in that paper), suggesting that it is possible that the flow structure and resulting time-dependence of the 'irregular' regime are associated more with nonlinear wave-wave interactions, rather than with wave-zonal flow interactions, but the latter interactions are by no means absent from the dynamics of the flow. In the present thermal topography case, however, there is very little correlation between the kinetic energy activity of the sum of the wavenumber components and the zonal mean flow. As such, wave-zonal flow interactions appear to have much less influence in the 'irregular' regime than in the 'interference' regime for thermal topography. Overall, therefore, throughout the entire examined parameter space of the experiments using thermal topography there seems to be evidence for a reduction in the impact of nonlinear wave-zonal flow interactions when compared to mechanical topography.

3.5. Vertical structure

The vertical structure of the Thermal Topography experiments, which are unblocked throughout, allows for a comparison with the vertical structure of Marshall and Read's (2018) Partial Barriers experiments, which had both blocked and unblocked sections. Figure 18 gives a snapshot of the vertical structure in the 'interference' regime, with each image taken roughly 10 seconds apart, to allow for construction of a streakline picture. Considering the slow drift speed and oscillation timescales, this was determined to be sufficiently frequent to represent measurements at all 5 levels as simultaneously as possible.

Figure 18 shows that the vertical structure of the experiments with thermal topography is typically more consistent over all five levels (notwithstanding an azimuthal shift with height) than that obtained with Marshall and Read's (2018) partial mechanical barriers (figure 20 in that paper). Instead of an azimuthally-localised wave at the bottom of the annulus, (a), (b) and (c) all show an irregular wavenumber-2 structure having just interacted with the topography, with a downstream (clockwise) shift with increasing height. This structure is familiar for this area of parameter space, also appearing in figure 9(a) at the bottom of the tank and figure 4(e) at mid-depth. Near the lid, as found for Marshall and Read's (2018) Partial Barriers experiments, the flow becomes weaker and more irregular, with both (d) and (e) appearing to show an irregular wavenumber-1 with reduced amplitude and evidence of being acted upon by higher wavenumbers, once more with a downstream shift and with the sloped lid appearing to suppress baroclinic activity.

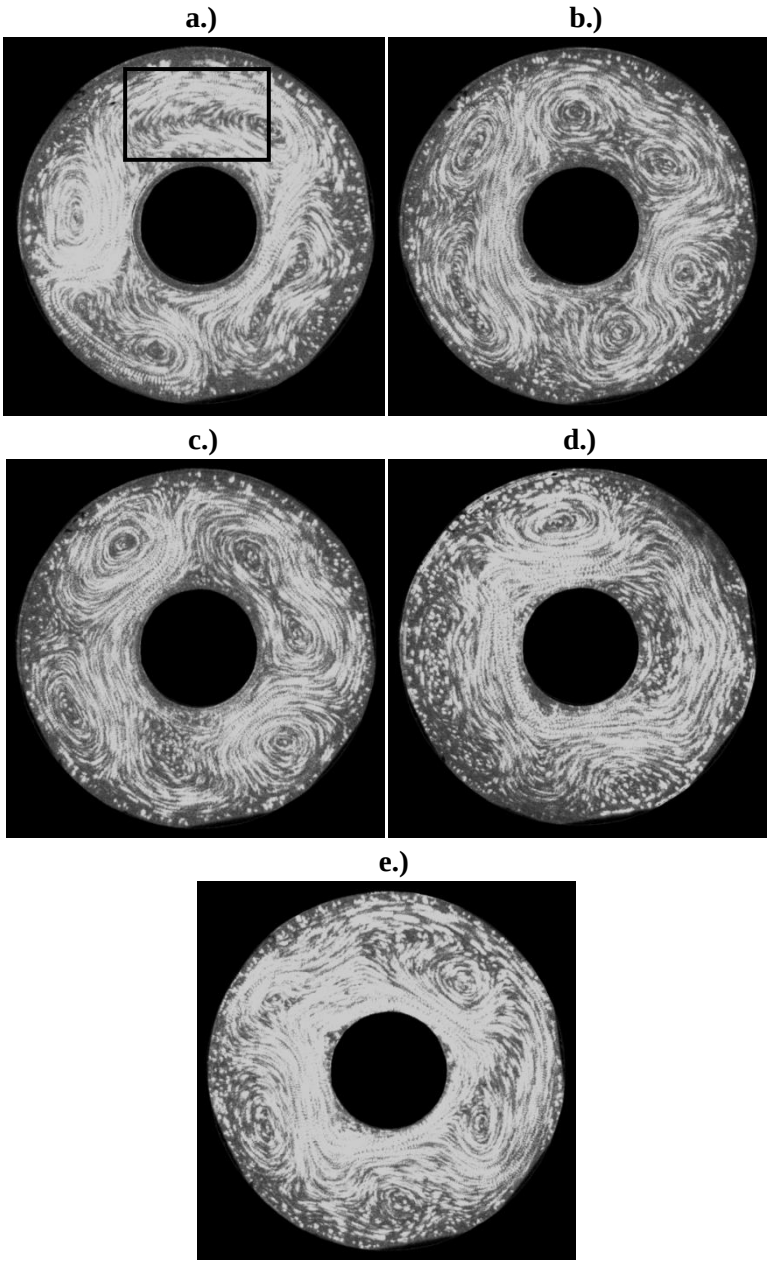

Figure 18: Sequence of almost simultaneous streakline images at each of five vertical levels at $\Omega = 1.0$ rads^{-1}, $\Delta T = 4$K, $\mathcal{T} = 5.680 \times 10^7$, $\Theta_T = 0.316$, a.) Level 5, b.) Level 4, c.) Level 3, d.) Level 2, e.) Level 2, f.) Level 1. Each image represents a 10s exposure to obtain the streak patterns, and is separated from the next image by 10s.

4. Discussion

Over the same regions of parameter space, the present Thermal Topography experiments and Marshall and Read's (2018) Partial Barriers experiments were both found to exhibit a number of similarities. In particular, azimuthally-varying heating in the annulus was indeed found to be able to replicate various aspect of flows and dynamics that were similar in form to those found with mechanical topography.

Most notably, both experiments evidently exhibit a lack of dominant stationary wave activity, both show evidence of topographic interactions and jet-shifting effects as the wave structures drift over the topographic peak or patch of heating elements, creating flows similar to the blocked and zonal states found with periodic bottom topography (such as found by Read and Risch 2011, Risch and Read 2015 and Marshall and Read 2015). Both systems were shown to have the same general shape of regime diagram, separated into two separate and distinct regions. The first was designated an 'interference' regime, found at low Taylor number, wherein a stationary wavenumber-1, mainly forced by the topography, interacted with the dominant drifting baroclinic wave and led to constructive or destructive interference which manifested itself in the form of radial jet-shifting, as the waves crossed the peak of the base.

The other main regime observed in both systems was an 'irregular' region, typically found at high Taylor number and small Hide number, where groups of resonant wave-triads were found to be associated with a transition toward more erratic and disordered types of flow. Both the isolated ridge and the thermal topography led to the formation of a coherent "butterfly" of Rossby-like waves, made up of two nonlinear resonant wave-triads sharing a common mode. In one set of cases, one triad was between the stationary wavenumber-1 component forced by the topography and drifting wavenumber-4 and wavenumber-5 components; the second triad was between the same stationary wavenumber-1 component forced by the topography and drifting wavenumber-5 and wavenumber-6 components. This would appear to indicate that the flows are dominated by nonlinear wave-wave interactions involving a

stationary wave forced by the topography. In addition, this also shows that resonant wave-triads can still occur with thermal topographic forcing and are not dependent on the precise forcing mechanisms associated with mechanical topography, as was put forward by Jin and Ghil (1990). Furthermore, since the wave-triad interactions act in the same way as for Marshall and Read's (2018) Partial Barriers experiment, and were associated with the occurrence of the 'irregular' regime in both studies, it is suggested that it is the general shape of the topography that determines whether the flow encounters a 'stationary-transition' regime and corresponding oscillations, as found with the wavenumber-3 topographic base of Marshall and Read (2015), or an 'irregular' regime.

These many similarities may act to somewhat verify the suggestion of Dickinson (1980), who showed evidence that planetary-scale waves should react to thermal topography in much the same way as to mechanical topography. Similarly, Kaspi and Schneider (2011) suggested that atmospheric cold anomalies observed on Eastern continental boundaries have associations with both topographic forcing and land-sea temperature differences, with each creating an impact similar in magnitude and effect.

The differences between flows found in the Thermal Topography and the Marshall and Read's (2018) Partial Barriers studies are twofold. Firstly, without any physical peak at the base, there is no blocked low-level circulation at the bottom of the annulus. This makes the vertical structure for the Thermal Topography experiments a lot more uniform, aside from a small shift downstream with height, as well as showing that the topographic interactions and 'interference' flows described here are independent of the presence of an azimuthally-trapped and stationary wave at the bottom of the tank. Secondly, the transition between the 'interference' and 'irregular' regimes as parameters are varied is significantly more gradual in the system with thermal topography, leading to more transitions between a wider range of wavenumbers, and stronger vacillations throughout.

4.1. Analysis of thermal topography experimental results

The results presented here agree well with the few experiments reported in the literature with azimuthally-varying heating. Boubnov, Golitsyn and Senatorsky (1991) found similar topographic interactions between the drifting baroclinic waves encountered in their experiments and the pattern of azimuthally-varying heating, in addition to noting evidence of nonlinear *blocking* effects, such as wave-wave interactions occurring along with a reduction in zonal flow. They also reported the presence of stationary wave regimes, which were not found in the current study. But this is likely the consequence of the location of the thermal topography - along the outer wall for their investigation, and attached to the base for the present experiments. Boubnov *et al.*'s (1991) experiment had a fully periodic topographic structure in azimuth, which was found (by Marshall and Read 2015, for example) to be more likely to produce stationary waves than the aperiodic isolated ridge from Marshall and Read's (2018) Partial Barriers investigation, from which the heating elements take their shape.

On the other hand, Jin and Ghil (1990) suggested that a thermally-forced study would not be expected to exhibit the same wave-zonal flow interactions as would be found with mechanical topography, due to the removal of form-drag effects, but would still be expected to exhibit wave-wave interactions. Whilst the occurrence of resonant wave-triads in our experiments do indeed give evidence of wave-wave interactions occurring with thermal topography, only a limited correlation between fluctuations in the kinetic energies of the zonal mean flow and the dominant wave was noted. Nonlinear wave-zonal flow interactions were therefore found to be reduced in importance in affecting the flow structure and evolution compared to the effects of wave-wave interactions, but not to be entirely absent, especially within the 'interference' regime found at higher Hide Number. This appears to contradict the suggestion from Jin and Ghil's numerical model, though it is possible that the weaker wave-zonal flow interactions from thermal topography are characteristically dissimilar enough to those generated by mechanical topography to be considered effectively distinct. This behaviour, as well as its causes and mechanism, should be investigated further in future work.

4.2 A Walker Circulation analogue?

Due to the similarities between the results of Marshall and Read's (2018) Partial Barriers and the present Thermal Topography experiments, we note a possible important analogy between our experiments and the Walker Circulation (WC) in the atmosphere, with a land-sea temperature difference on the order of the polar-Equator temperature difference producing comparable flow patterns to that of a major mountain range. The WC, in the case of the Thermal Topography study, was believed to be apparent in the form of jet-shifting interference effects. When the flow is not interacting with the thermal topography (i.e. the immediate temperature difference is lower) the zonal state with a strong jet occurs, and when the flow does interact with the thermal topography (i.e. the immediate temperature difference is higher) a blocked state with a reduced strength jet is found. This agrees well with the findings of Bjerknes (1969), wherein the strength of the WC was found to be stronger when the corresponding sea-surface temperatures were lower, and weaker when they were higher. In addition, Julian and Chervin (1978) noted that the atmospheric impact of the land-sea temperature difference is felt westward (i.e. downstream) of the peak heat source. In the same way, the jet-shifting phenomenon of the Thermal Topography study was found to always occur downstream of the heating elements. Assuming that the observed phenomena are indeed analogous to the WC, this would be the first time the WC has been so thoroughly replicated in a differentially-heated annulus.

These results also possibly suggest that the El Niño Southern Oscillation (ENSO) which, as discussed in Philander (1985), is a chaotic oscillation between periods of warming (El Niño) and cooling (La Niña) of the Pacific tropics with a timescale on the order of 3-6 years, could have some relationship with the frequent transitions and strong vacillation of many of the flows found, or may occur as the equivalent of the onset of the 'irregular' regime. However, the real ENSO is more complicated than this, as it involves coupled oscillations in both the oceans and the atmosphere interacting with each other.

4.3. Climate change

As discussed in Marshall and Read (2018), there are many recent publications that deal with atmospheric climate change, with a number suggesting that severe weather events are due to a rise in number and longevity of persistent blocked events and stationary waves. Of these, Power and Smith (2007), Francis and Vavrus (2012) and Liu *et al.* (2012) all put forward that the persistent blocked events are due to decreased atmospheric thermal topography, as a result of a reduction in sea-ice from climate change. The results of the Thermal Topography investigation appear to agree with this proposal, albeit in an indirect manner, as the impacts on the large-scale flow from azimuthally-varying heating were found to be comparable to that from mechanical topography, and a reduction in this forcing would be expected to lead to significant changes to atmospheric LFV and the global circulation, as discussed previously. Further experiments with varying amounts of heat input would be needed to investigate this further, however.

4.4. Geothermal activity

In the ocean circulation, thermal topography can arise from geothermal activity caused by volcanoes. In this case, the impact of geothermal heat flux at the ocean bottom is a reduction of stratification throughout the abyssal layer, resulting in a strengthening of the circulation, as observed by Mashayek *et al.* (2013). In the present Thermal Topography experiments, the heat influx from the heating elements created an impact similar to that of the mechanical topography of Marshall and Read's (2018) Partial Barriers experiment, and thus could indeed be described as causing a strengthening of the circulation, in the form of baroclinic waves and interference effects. In contrast to the mechanical topographic study, however, the experiments with azimuthally-varying heating were found to be noticeably more uniform in the vertical direction, with the flow structure changing only slightly with height. Due to this, the results of the Thermal Topography experiments appear qualitatively to capture

many of Mashayek *et al*.'s proposed effects of a geothermal heat flux on the oceanic flow, though a more in-depth further investigation would be required to fully verify these impacts under more comprehensively realistic conditions. In addition, the observed similarity to mechanical topography also backs up the suggestion that geothermal heat flux may be a significant component for inclusion into oceanic modelling, at least locally.

4.5. The Martian atmosphere

On Mars, the atmospheric linear stationary response is quite different to that of the Earth, as noted in the numerical studies of Webster (1977) and Hollingsworth and Barnes (1995), and in observations, such as from Banfield *et al.* (1996). The Martian atmosphere is found to be dominated by low wavenumber disturbances, in turn linked to the formation of robust stationary eddies (and hence, also contributing to the development of global dust storms, as discussed earlier) in the Martian atmosphere, especially in the Northern Hemisphere. Hollingsworth and Barnes, amongst others, suggested that these disturbances are due to the Martian surface acting as both topographic and thermal forcing. In the Thermal Topography experiments, the regime diagram shows that lower wavenumbers were slightly more common than in the Marshall and Read's (2018) similar Partial Barriers experiments, especially at low Taylor Numbers and high Hide Numbers. In this way, it is possible that it is indeed the Martian thermal forcing that leads to low wavenumber flow structures, but this could only be fully verified by further experiments using a combination of mechanical and thermal topography, such as by attaching flat heating elements to the topographic peaks.

Acknowledgements

S.D. Marshall was funded by partial doctoral training awards respectively from the UK National Environment Research Council and Science and Technology Facilities Council. PLR acknowledges support from STFC grants ST/I001948/1 and ST/K00106X/1, and EPSRC grant EP/K029428/1. The authors would like to thank the reviewers of this paper for providing detailed and constructive comments and suggestions.

References

Banfield, D., Toigo, A.D., Ingersoll, A.P. and Paige, D.A., Martian weather correlation length scales. *Icarus 1996,* **119**(1), 130-143.

Bjerknes, J., Atmospheric teleconnections from the equatorial Pacific. *Mon. Wea. Rev.* 1969, **97**(3), 163-172.

Boubnov, B.M., Golitsyn, G.S. and Senatorsky, A.O., Convection in a rotating cylindrical annulus with azimuthally non-uniform heating. *Geophys. Astrophys. Fluid Dyn.* 1991, **57**(1), 1-18.

Bretherton, F.P., Resonant interactions between waves. The case of discrete oscillations. *J. Fluid Mech.* 1964, **20**(3), 457-479.

Charney, J.G. and DeVore, J.G., Multiple flow equilibria in the atmosphere and blocking. *J. Atmos. Sci.* 1979, **36**(7), 1205-1216.

Cho, J.Y.K., Atmospheric dynamics of tidally synchronized extrasolar planets. *Phil. Trans. R. Soc. Lond. A* 2008, **366**(1884), 4477-4488.

Dickinson, R.E., Planetary waves: Theory and observation. In WMO, *Orographic Effects in Planetary Flows*, GARP Publ. Ser.23 1980, 23, 51-84.

Fincham, A.M. and Spedding, G.R., Low cost, high resolution DPIV for measurement of turbulent fluid flow. *Exp. Fluids* 1997, **23**(6), 449-462.

Fowlis, W.W. and Hide, R., Thermal convection in a rotating annulus of liquid: Effect of viscosity on the transition between axisymmetric and non-axisymmetric flow regimes. *J. Atmos. Sci.* 1965, **22**, 541-558.

Francis, J.A. and Vavrus, S.J., Evidence linking Arctic amplification to extreme weather in mid-latitudes. *Geophys. Res. Lett.* 2012, **39**(6).

Früh, W-G. and Read, P.L., Wave interactions and the transition to chaos of baroclinic waves in a thermally driven rotating annulus. *Phil. Trans. Math. Phys. Eng. Sci.* 1997, **355**(1722), 101-153.

Georgen, J.E. and Lin, J., Three-dimensional passive flow and temperature structure beneath oceanic ridge–ridge–ridge triple junctions. *Earth Planet. Sci. Lett.* 2002, **204**(1-2), 115-132.

Glycerine Producers' Association, *Physical Properties of Glycerine and its Solutions*. New York: Glycerine Producers' Association 1963.

Hide, R., An experimental study of thermal convection in a rotating liquid. *Phil. Trans. R. Soc.Lon. A* 1958, **250**(983), 441-478.

Hide, R. and Mason, P.J., Sloping convection in a rotating fluid. *Adv. Phys.* 1975, **24**(1), 47-100.

Hollingsworth, J.L. and Barnes, J.R., Forced stationary planetary waves in Mars's winter atmosphere. *J. Atmos. Sci.* 1996, **53**(3), 428-448.

Holton, J.R., *An Introduction to Dynamic Meteorology.* 3rd ed. New York: Academic Press 1992.

Jin, F.F. and Ghil, M., Intraseasonal oscillations in the extratropics: Hopf bifurcations and topographic instabilities. *J. Atmos. Sci.* 1990, **47**(24), 3007-3022.

Julian, P.R. and Chervin, R.M., A study of the Southern Oscillation and Walker Circulation phenomenon. *Mon. Wea. Rev.* 1978, **106**(10), 1433-1451.

Kartashova, E. and L'vov, V.S., Model of intraseasonal oscillations in Earth's atmosphere. *Phys. Rev. Lett*. 2007, **98**(19), 198501(4).

Kaspi, Y. and Schneider, T., Winter cold of eastern continental boundaries induced by warm ocean waters. *Nature* 2011, **471**, 621–624.

Li, G., Kung, R. and Pfeffer, R.L., A fluid experiment of large-scale topography effect on baroclinic wave flows. *Adv. Atmos. Sci.* 1992, **9**(1), 17-28.

Liu, J., Curry, J.A., Wang, H., Song, M. and Horton, R.M., Impact of declining Arctic sea ice on winter snowfall. *Proc. Natl. Acad. Sci. USA* 2012, **109**(11), 4074-4079.

Marshall, S.D. and Read, P.L., An experimental investigation into topographic resonance in a baroclinic rotating annulus. *Geophys. Astrophys. Fluid Dyn.* 2015, **109**(4), 391-421.

Marshall, S.D. and Read, P.L., Blocking by partial barriers: An experimental investigation in a baroclinic rotating annulus. *Geophys. Astrophys. Fluid Dyn.* 2018, **112**(2), 97-129.

Mashayek, A., Ferrari, R., Vettoretti, G. and Peltier, W.R., The role of the geothermal heat flux in driving the abyssal ocean circulation. *Geophys. Res. Lett.* 2013, **40**(12), 3144-3149.

Mason, P.J., Baroclinic waves in a container with sloping end walls. *Phil. Trans. R. Soc. Lond. A* 1975, **278**(1284), 397-445.

Meehl, G.A., Coupled land-ocean-atmosphere processes and South Asian monsoon variability. *Science* 1994, **266**(5183), 263-267.

Nayvelt, L., Gierasch, P.J. and Cook, K.H., Modeling and observations of Martian stationary waves. *J. Atmos. Sci.* 1997, **54**(8), 986-1013.

Pedlosky, J., *Geophysical Fluid Dynamics*. 2nd ed. New York and Berlin: Springer-Verlag 1987.

Philander, S.G.H., El Niño and La Niña. *J. Atmos. Sci.* 1985, **42**(23), 2652-2662.

Power, S.B. and Smith, I.N., Weakening of the Walker Circulation and apparent dominance of El Niño both reach record levels, but has ENSO really changed? *Geophys. Res. Lett.* 2007, **34**(18).

Read, P.L., Bell, M.J., Johnson, D.W., and Small, R.M. Quasi-periodic and chaotic flow regimes in a thermally driven, rotating fluid annulus. *J. Fluid Mech.* 1992, **238**, 599-632.

Read, P.L. and Lewis, S.R., *The Martian Atmosphere Revisited: Atmosphere and Environment of a Desert Planet*. Chichester: Praxis Publishing Ltd 2004.

Read, P.L. and Risch, S.H., A laboratory study of global-scale wave interactions in baroclinic flow with topography, Part I: Multiple flow regimes. *Geophys. Astrophys. Fluid Dyn.* 2011, **105**(2-3), 128-160.

Read, P.L., Pérez, E.P., Moroz, I.M. and Young, R.M.B., General circulation of planetary atmospheres: Insights from rotating annulus and related experiments, in *Modeling Atmospheric and Oceanic Flows: Insights from Laboratory Experiments and Numerical Simulations (eds. T. von Larcher and P. D. Williams)*, AGU and Wiley, New Jersey USA 2015, 9-44.

Risch, S.H. and Read, P.L., A laboratory study of global-scale wave interactions in baroclinic flow with topography, Part II: Vacillations and low-frequency variability. *Geophys. Astrophys. Fluid Dyn.* 2015, **109**(4), 359-390.

Shulmeister, J., Australasian evidence for mid-Holocene climate change implies precessional control of Walker Circulation in the Pacific. *Quat. Int.* 1999, 57, 81-91.

Taylor, G.I. Stability of a viscous liquid contained between two rotating cylinders. *Phil. Trans. R. Soc. Lon. A* 1923, **223**(612), 289-343.

Webster, P.J., The low-latitude circulation of Mars. *Icarus* 1977, **30**(4), 626-649.

Weeks, E.R., Tian, Y., Urbach, J.S., Ide, K., Swinney, H.L. and Ghil, M., Transitions between blocked and zonal flows in a rotating annulus with topography. *Science* 1997, **278**(5343), 1598-1601.

Wordsworth, R.D., Read, P.L. and Yamazaki, Y.H., Turbulence, waves, and jets in a differentially heated rotating annulus experiment. *Phys. Fluids* 2008, **20**(12), 126602.